Research Square

Preprints are preliminary reports that have not undergone peer review.
They should not be considered conclusive, used to inform clinical practice,
or referenced by the media as validated information.

Identification of Plant-Based Drug-like Molecules as Potential Inhibitors against hACE2 and S-RBD of SARS-CoV-2 using Multi-step Molecular Docking and Dynamic Simulation Approach.

Arpana Parihar (arpana_parihar@yahoo.com)
CSIR-Advanced Materials and Processes Research Institute (AMPRI)

Zannatul Ferdous Sonia
The Red-Green Research Centre, BICCB, 16 Tejkunipara, Tejgaon, Dhaka, 1215, Bangladesh

Nishant kumar Choudhary
NIMS University, Jaipur

Palak Sharma
NIMS University, Jaipur

Iktedar Mahdi
The Red-Green Research Centre, BICCB, 16 Tejkunipara, Tejgaon, Dhaka, 1215, Bangladesh

Fuad Taufiqul Hakim Hakim
The Red-Green Research Centre, BICCB, 16 Tejkunipara, Tejgaon, Dhaka, 1215, Bangladesh

Md Ackas Ali
The Red-Green Research Centre, BICCB, 16 Tejkunipara, Tejgaon, Dhaka, 1215, Bangladesh

Raju Khan
CSIR-Advanced Materials and Processes Research Institute (AMPRI)

Mohammed S. Alqahtan
King Khalid University

Mohamed Abbas
King Khalid University

Article

Keywords: SARS-CoV-2, Phytochemicals, S-RBD/hACE2, In-Silico screening, Molecular Docking & simulation, COVID-19

Posted Date: April 7th, 2022

DOI: https://doi.org/10.21203/rs.3.rs-1517448/v1

License: This work is licensed under a Creative Commons Attribution 4.0 International License.
Read Full License

Identification of Plant-Based Drug-like Molecules as Potential Inhibitors against hACE2 and S-RBD of SARS-CoV-2 using Multi-step Molecular Docking and Dynamic Simulation Approach.

Arpana Parihar[1*], Zannatul Ferdous Sonia[2], Nishant Kumar Choudhary[3], Palak Sharma[3], Iktedar Mahdi[2], Fuad Taufiqul Hakim[2], Md Ackas Ali[2], Raju Khan[1,4*], Mohammed S. Alqahtan[5,6], and Mohamed Abbas[7,8]

[1]Industrial Waste Utilization, Nano and Biomaterials, CSIR-Advanced Materials and Processes Research Institute (AMPRI), Hoshangabad Road, Bhopal-462026, MP, India

[2]Division of Infectious Diseases and Division of Computer-Aided Drug Design, The Red-Green Research Centre, BICCB, 16 Tejkunipara, Tejgaon, Dhaka, 1215, Bangladesh

[3]NIMS Institute of Allied Medical Science and Technology, NIMS University, Jaipur- 303121, Rajasthan, India

[4]Academy of Scientific and Innovative Research (AcSIR), Ghaziabad-201002, India

[5]Radiological Sciences Department, College of Applied Medical Sciences, King Khalid University, Abha 61421, Saudi Arabia.

[6]BioImaging Unit, Space Research Centre, Michael Atiyah Building, University of Leicester, Leicester, LE1 7RH, U.K.

[7]Electrical Engineering Department, College of Engineering, King Khalid University, Abha 61421, Saudi Arabia.

[8]Computers and communications Department, College of Engineering, Delta University for Science and Technology, Gamasa 35712, Egypt.

*__Corresponding Author:__ Arpana Parihar (arpana_parihar@yahoo.com), Raju Khan (khan.raju@gmail.com)

Abstract

There has been considerable interest to develop effective antiviral drugs with substantial efficacy to the varying lineage of SARS-CoV-2. The plant-based bioactive molecules (phytochemicals) have proven to exhibit promising therapeutic efficacy and immune-modulatory effect due to their inherent broad-spectrum biological properties such as antioxidant, antiviral, and anti-inflammatory with minimal or no side effects. The SARS-CoV-2 infection is initiated upon recognition and binding of the spike (S) Receptor-Binding Domain (RBD) to the host cell surface receptor, human Angiotensin-Converting Enzyme 2 (hACE2). Therefore, the underlying mechanism of interaction between host cell receptors and blocking the virus-cell interaction is considered to be a promising approach for the management and treatment of COVID-19 disease. In the present study, *In-silico* screening of phytochemicals against two targets of SARS-CoV-2 using a multi-step molecular docking approach was investigated. Based on the Glide-XP docking score, the top 5 molecules were subjected to steered molecular dynamics (SMD) simulation for calculation of binding force, and work done to get mechanistic insight has been carried out. Further, the op 3 ligands with the highest force and work were subjected to molecular dynamics simulation and binding free energy evaluations. The results revealed that the protein-ligand complexes showed stable trajectories throughout the 100 ns simulation. Moreover, the drug likeliness predicted by pKi, LE, ADMET analysis, and Pa & Pi values suggested that the best 3 lead molecules for both the targets (ACE2: Rosavin, Isoorientin, Palasitrin) & (RBD: Cinnamtannin B1, Isoskimmiwallin, Terflavin A) have good inhibitory efficiency, better pharmacokinetics, and are non-toxic under physiological conditions. Thus, these molecules can be used as potential therapeutic drugs against SARS-CoV-2 infection.

Keywords: SARS-CoV-2, Phytochemicals, S-RBD/hACE2, *In-Silico* screening, Molecular Docking & simulation, COVID-19.

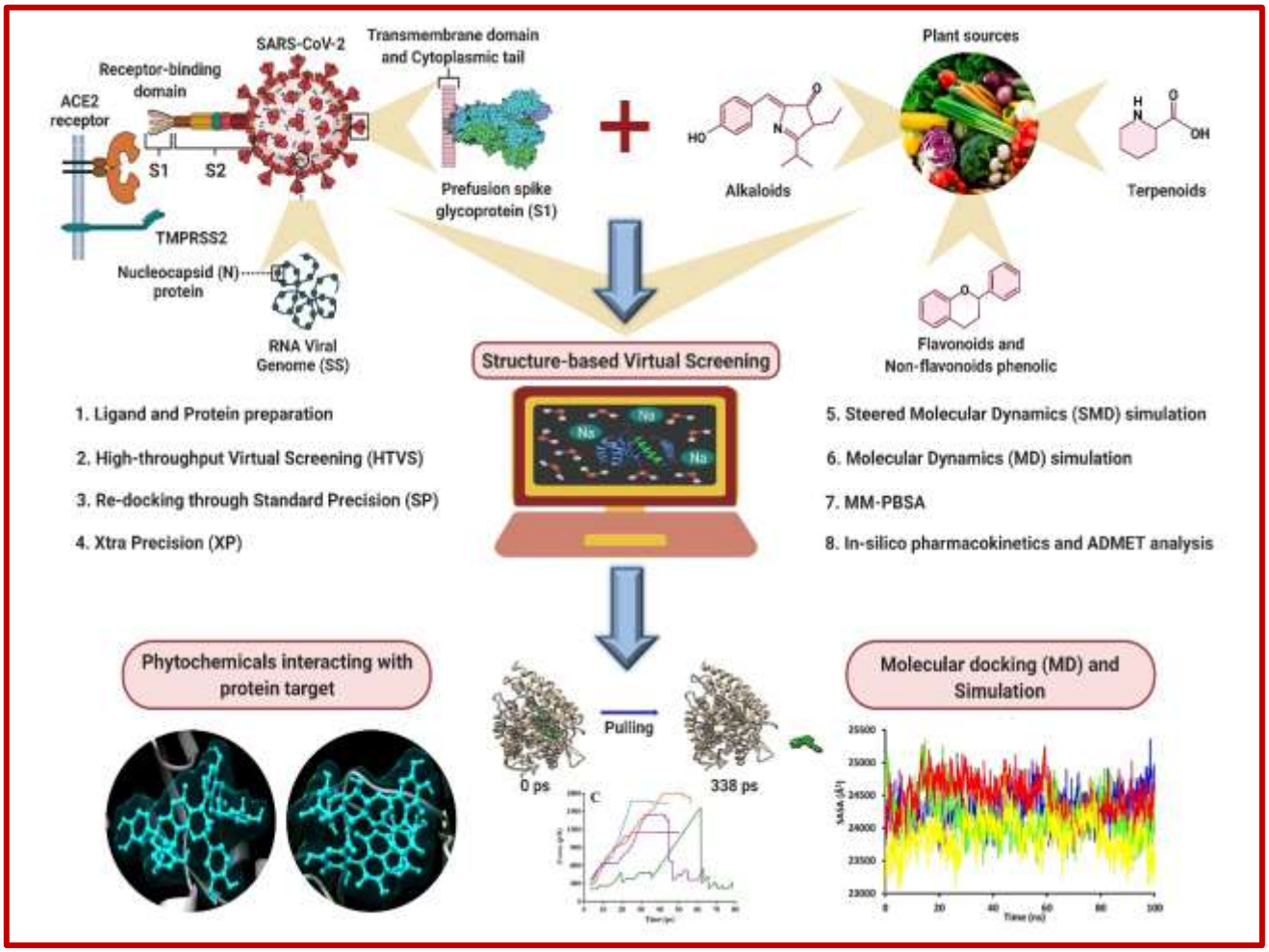

Graphical Abstract

1. Introduction

The coronavirus disease (COVID-19) caused by the novel coronavirus SARS-CoV-2 is termed as severe acute respiratory syndrome coronavirus 2, which emerged as a global pandemic threat to human beings and caused widespread concerns due to its contagiousness, fatality rate, and the absence of drug(s)[1]. Beta-CoVs or β-CoVs are among the four genera: Alpha (B.1.1.7), Beta (B.1.351), Gamma (GR/501Y.V3 or P.1), and Delta (B.1.617.2) of coronaviruses which are enveloped, positive-strand RNA viruses that infect mammals composed of varying viral lineages[2]. The Beta variant (20H/501Y.V2 or B.1.351) is a variant of SARS-CoV-2, the virus that causes the COVID-19 outbreak. Among these, α and β-CoVs causes infection to mammals whereas, γ and δ-CoVs tend to infect birds[3]. On February 11, 2020, the "International Committee on Taxonomy of Viruses" adopted the official name for SARS-CoV-2. The World Health Organization (WHO) labelled the variant as a Beta variant and tagged it as a Variant of Concern (VOC)[4]. Recently, a new variant named Omicron (B.1.1.529) has been reported by WHO from South Africa on November 24, 2021, upon recommendation of the Technical Advisory Group on Virus Evolution (TAG-VE)[5]. Initial investigation suggests that Omicron displayed a 13-fold increase in viral infectivity, and is 2.8 times more infection rate than the Delta variant. As per the report, UK Health Security Agency (UKHSA) has classified a new Omicron subtype (BA.2), which is spreading quickly and could be even more contagious, and tagged this lineage as Variant under Investigation (VUI-22JAN-01)[6].

As a novel Betacoronavirus, SARS-CoV-2 shares 79% genome sequence identity with Severe Acute Respiratory Syndrome Coronavirus 1 (SARS-CoV-1 or SARS-CoV) and 50% with the Middle East Respiratory Syndrome Coronavirus (MERS-CoV), the respiratory illness responsible for the 2002–2004 SARS outbreak[7,8]. The COVID-19 outbreak has become a major public health concern because of the higher associated mortality and morbidity rate around the world. In grievous conditions, it may cause Acute Respiratory Distress Syndrome (ARDS) which is a different form of respiratory anomalies associated with the condition in which fluid collects in the air sacs of the lungs, resulting in septic shock and depriving organs of oxygen[9]. The jeopardy of death increases with the age and severity of illness. Globally, February 23, 2022, there have been 426,624,859 confirmed cases of COVID-19, including 5,899,578 confirmed deaths[10]. Due to the high rate of spontaneous mutation in SARS-CoV-2, certain vaccines and drugs have proven their propitious and potency but with a varying degree of intolerance and complications[11].

Coronavirus contains a non-segmented, positive-sense RNA genome of ~30 kb. The genome contains a 5′ cap structure along with a 3′ poly (A) tail. Thus, allowing it to act as an mRNA for translation of the replicase polyproteins[12]. The virus genome encodes twenty different proteins including four main structural proteins, two polyproteins (pp1a and pp1ab), possibly nine accessory proteins (ORF3a, 3d, 6, 7a, 7b, 8, 9b, 14 & 10), and many non-structural proteins including coronavirus main protease (3CLpro or Mpro), RdRp (nsp12-nsp7-nsp8 complex) and PLpro[13]. The structural proteins of SARS-CoV-2 consist of (S) Spike protein (~150 kDa), (M) Membrane protein (~25–30 kDa), (E) Envelope protein (~8–12 kDa), and (N) Nucleocapsid protein (~0.7 kDa)[14]. The nucleocapsid (N) protein plays an essential role both in the viral

genomic RNA packaging and the regulation of host cellular machinery[15]. Cellular infection and replication cycle by the SARS-CoV-2 depends upon the host protein (ACE2) Angiotensin-Converting Enzyme 2 receptor[16]. ACE2 is a transmembrane glycoprotein consisting of 805 amino acids and contains two homologous domains: the amino-terminal catalytic domain and the carboxy-terminal domain[17]. The catalytic domain has one active site – the zinc metallopeptidase domain, which shows ~42% sequence identity with the amino domain of ACE[18]. The spike (S) protein of SARS-CoV-2 mediates entry by binding to the ACE2 receptor present on the cell surface followed by fusion of the viral envelope with the host cell membrane[19]. The S protein consists of two subunits: S1 and S2, where the S1 subunit is responsible for receptor binding consisting Receptor-Binding Domain (RBD) whereas, S2 is responsible for membrane fusion[20,21]. RBD is a short immunogenic fragment from a virus that binds to the specific endogenous receptor sequence, to attain entry into the host cells. Further, it also requires priming of the virus spike protein by the Trans-Membrane Protease Serine 2 (TMPRSS2), which cuts the spike protein in a specific location[22]. Then, it undergoes a series of dramatic conformational changes. During the first stage, the spike protein inserts into the cell membrane, and once inserted, the spike protein folds back on itself, pulling the membrane of the cell and virus together so that they can fuse easily. After fusion, the viral RNA is deposited into the host cell where it hijacks the cell's machinery to produce more viruses[23]. The binding affinity between the ACE2 receptor and the space outside a cell, which leads to signal transduction (ectodomain structure) of the S protein, determines the human transmission capability and the inflammatory responses[24].

Current global cascades have reportedly engaged medical sciences in the discovery of potent therapies and drugs which has supreme efficacy. But no ideal solutions have been discovered yet. Use of certain antiviral drugs and immunomodulation therapies such as Remdesivir, Ivermectin, Lopinavir-Ritonavir, Hydroxychloroquine, etc., along with certain supplements of micronutrients and vitamins is being used for the treatment of COVID-19 diseases[25,26]. These drugs have a varied range of side effects and responses on particular individuals. The high consumption and overall demand, it has resulted in limited supply which creates havoc among the people. Therefore, one of the alternative broad therapeutic spectra against COVID-19 virus infection is the search for plant-based natural enzyme inhibitors using virtual screening, to obtain drugs with minimal side effects[27–31]. The flavonoids and non-flavonoid phenolic, terpenes, and alkaloids are explored as promising therapeutic class having potential antiviral activities due to their inherent properties such as antioxidant, immunomodulatory, and anti-inflammatory roles that could reduce the severity of infection, disease symptoms and enhance the immune response of the patient[32–34]. Recent studies reported the antiviral activity of plant-based phytochemicals to bind with SARS-CoV-2 spike protein and ACE2 receptor[35].

The implication of computational biology has opened a new gateway in the vicinity of drug designing and development. Molecular docking is a key technique to foresee ligands' binding capacity and interactions to design drugs[36]. In this work, High-Throughput Virtual Screening (HTVS) is carried out to search potent antiviral molecule among ~1000 phytochemicals against two druggable targets ACE2 receptor and spike

RBD protein. The virtual screening and pharmacokinetics results help to study the interaction as well as the role of a bioactive compound in various biochemical process, at the cellular level and provide a preceding aim for drug design development[37]. For selecting the best molecules (ligands/compounds) based on conformational flexibility, charges distribution, and solvent role in target recognition and binding, we performed molecular modeling-based methods which include multistep Molecular Docking, Steered Molecular Dynamics (SMD) simulation, Molecular Dynamic (MD) simulation followed by Molecular Mechanics-Poisson Boltzmann Surface Area (MM-PBSA) calculations. The study revealed, five (5) potential phyto-molecules for both the targets ACE2 (Eriocitrin, Rosavin, Isoorientin, Palasitrin, and Ascorbic Acid) & RBD (Procyanidin C1, Tannic Acid, Cinnamtannin B1, Isoskimmiwallin and Terflavin A). These molecules have shown a strong ability to bind with the receptor-binding site with high docking scores, high binding energy, close interactions and acting as a potential inhibitor by preventing ACE2 and RBD interaction. Their non-bonding interactions with the protein residues were also investigated. The result is concluded based on pulling force (directional) and work done estimated by steered molecular dynamic simulation. The MM-PBSA binding free energy calculations and non-bonding interaction studies along molecular dynamic simulation results further confirmed that these phyto-molecules (ligands) formed stable complex with their respective targets. Moreover, the ADMET profile and pharmacokinetics study of lead molecules revealed their better drug likeliness and antiviral properties. However, their pre-clinical optimization may be necessary which can be examined *via In-vivo* or *In-vitro* experimental studies before considering them as therapeutic measures for SARS-CoV-2.

2. Materials and Methods

In this research, a wide range of plant-based phytochemicals has been screened as potential inhibitors using computer-assisted virtual screening (computational approach) against ACE2 receptor and spike RBD of SARS-CoV-2. Earlier, the selection of lead compounds in drug discovery from identification to clinical trial was a cost expensive and time-consuming process[38]. Due to the recent advancement in computational biology, the virtual screening of certain bioactive compounds has become a gold standard technique, in drug designing and development for a specific target via the Maestro Schrodinger suite[39]. Several advanced approaches like multi-step molecular docking, steered molecular dynamic simulation, binding free energy calculation using the MM-PBSA approach, *in-silico* assessment, and MD simulation was carried out to select the best molecules with high potential antiviral activities against both the targets (ACE2 and RBD).

2.1. Ligands and Protein preparation:

A total of ~1000 phytomolecules (ligands) were retrieved from the PubChem database in a Structured Data Format (.sdf). These molecules are the bio-active natural compound that has been selected, based on their chemical-like properties[40]. These compound has been chosen based on earlier evidence for acting as an antiviral agent against various human pathogenic viruses. The three-dimensional (3D) chemical structures/conformers of the selected ligands are prepared and optimized by the removal of water molecules,

addition of the polar hydrogen atoms, 3D protonation followed by energy minimization, before using these molecules for molecular modelling process. Ligand Preparation (LigPrep) module of Schrodinger suite set on default parameters was considered to prepare the molecules. The Epik tool was applied to produce the protonation states of the molecules at physiological pH of 7.4[41]. These optimized ligand structures were then saved into Protein Data Bank (.pdb) file format for further indagation.

The 3D X-ray crystallographic structures of SARS-CoV-2, inhibitor bound with Human Angiotensin-Converting Enzyme-Related Carboxypeptidase (ACE2) and spike receptor-binding domain (RBD) was retrieved from the RCSB Protein Data Bank (PDB) (PDB ID: 1R4L & 6M0J). The two important parameters for both the targets such as resolution (1R4L: 3.00 Å) & (6M0J: 2.45 Å) and R-value (1R4L: 0.337) & (6M0J: 0.227) of the protein were checked respectively. The amino acid sequence length of both the protein are 615 & 603 respectively[42]. Schrodinger's Protein Preparation Wizard tool was used to add Hydrogen atoms and charges to the proteins while protein preparation. The co-crystallized water molecules were removed. A set of parameters associated with the connectivity of molecules were examined and ensured the correct metal ionization states, bond order, formal charges, and capping of the protein terminal with ACE and NMA residues[43]. The added hydrogen atoms were optimized via the protein's H-bonding network employing a systematic and cluster-based approach. We have used the PROPKA module of the Protein Preparation Wizard tool to determines the protonation state of the protein at a physiological pH 7.4. Finally, protein molecules were prepared by applying molecular mechanics force field (OPLS3e) to minimize the energy for each configuration and allow for sufficient heavy-atom movement to reduce strained bonds, angles, and clashes[44]. The Receptor Grid Generation (RGG) panel of the Glide (Grid-Based Ligand Docking with Energetics) module of the Schrodinger suite interface was used to generate the grid. Hence, the Grid box dimension was considered as 20 × 20 × 20 Å along X-, Y- and Z-axes. Now, the selected target protein was used as a receptor for virtual screening using multi-step molecular docking.

2.2. Virtual screening using multi-step molecular docking:

The structure-based virtual screening (SBVS) method is widely used in drug discovery. The Virtual Screening Workflow (VSW) module available in the Schrodinger suite was accounted to screen the potential molecule from the library made from the PubChem database. The VSW tool is projected to run an entire sequence of jobs for screening large collections of phyto-compounds against one or more receptor targets. Machine learning algorithms were extensively used in virtual screening techniques. The VSW utility program is unified with the subsequent multi-step molecular docking that includes Glide-HTVS (High-Throughput Virtual Screening), Glide-SP (Standard Precision), and Glide-XP (Xtra Precision)[45,46]. Emodel scoring is one of the salient molecular docking scoring functions and was used by the Glide algorithm of the Schrodinger suite which picks up the best suitable ligands. The GlideScore acts as an important tool to separate active and inactive small molecules with strong binding affinity from those with little or no binding interactions[47]. In every successive step of docking, a standardized approach was carried out to achieve the

best orientation of the molecule. The QikProp module was determined to exclude the molecules violating pharmaceutical-like properties, ADME (Absorption, Distribution, Metabolism & Excretion), and Lipinski's rule of five (LoF)[48]. In this study, High-Throughput Virtual Screening (HTVS) is carried out for 1000 phytomolecules with potential antiviral activities for both the targets (1R4L and 6M0J). Among them, the top 100 molecules for both targets are selected based on binding affinity. A standard protocol [Re-docking through Standard Precision (SP)] was carried out for the remaining compounds, among them the top 20 molecules were selected. Similar to the previous step followed by the selection of the top 5 docked molecules through Xtra Precision (XP). The lead molecules were subjected to Steered Molecular Dynamics (SMD) simulations followed by 100 ns of molecular dynamic simulation and Molecular Mechanics-Poisson Boltzmann Surface Area (MM-PBSA) binding free energy calculations[49]. Based on high docking score (ΔG° in kcal/mol), lowest inhibition/dissociation constant (Ki in nm), high binding free energy, and non-bonding interactions these top-ranked molecules were further evaluated for pharmacokinetic behavior.

The following equation is employed to calculate Ki,

$$Ki = exponential\left(\frac{\Delta G^{\circ}}{RT}\right)$$

Where,

R = universal gas constant (1.987 Kcal mol^{-1})

T = temperature (298.15 K)

Ligand efficiency (LE) is a commonly applied parameter for lead selection by comparing the values of average binding energy per atom[50].

The following formula was applied to calculate LE,

$$LE = -\Delta G/N$$

Where,

LE = ligand efficiency (kcal mol^{-1} non-H $atom^{-1}$)

ΔG = represents binding affinity (kcal mol^{-1})

N =number of non-bond H-atoms in the ligand

2.3. Steered Molecular Dynamics (SMD) simulation:

Harmonic time-dependent dynamics on the protein−ligand complex using steered molecular dynamics simulation which is based on standard Hamiltonian method was performed. A time-dependent external force was exerted to the ligand in order to dissociate it from the protein-ligand complex. In this study, the YASARA steered molecular dynamics protocol is chosen to perform the simulation[51].

The chosen top 5 protein-ligand complexes against each protein target (PDB IDs: 1R4L, ACE2 receptor; 6M0J, spike receptor-binding domain) was subjected to SMD. The complexes were selected based on their

docking results. A physiological environment was generated under the AMBER14 force field[52], the solvent density of 0.997 g/cm3 (water solvent), Na+/Cl^- ions of 0.9%, and pH of 7.4 at temperature 298K were incorporated. To execute the simulation, a Periodic boundary condition was employed where cuboid box size for both proteins was chosen. The initial energy minimization was performed applying the steepest gradient approach (5000 cycles). The temperature was controlled using the Berendsen thermostat and the pressure was kept constant throughout the whole simulation process. The overall equilibration time was 3 ps. In this protocol, the acceleration was kept 200ps. The starting and minimum pulling acceleration were chosen to 200 pm/ps2 (picometer/picosecond squared). The acceleration was applied at the centre of mass of the ligand, while the axis was formed by the centre of mass of the protein cavity. This protocol also provides the force value concerning the time of simulation and the distance value of dislocation. The average force profile (F) of 3 individual runs for each protein-ligand complex was calculated by Eqn. (i). Work (W) was also calculated using Eqn. (ii) until the point beyond no interactions existed between the ligand-protein complexes. The g(x) is obtained from the output of the YASARA protocol and x_{dissc} was obtained by observing the (.pdb) files via Discovery Studio Visualizer, and finding the time at which complete dissociation occurs, the corresponding distance, i.e. x_{discc} is collected from the YASARA output data file. To automate this process of work an in-house script is generated in OCTAVE was used. The 30 Å for 1R4L and 20 Å for 6M0J pulling length were defined, which ensured the complete dissociation and solvation of the ligand. Generally, this SMD protocol runs until the time needed to reach the system at the defined distance. In particular, a time phase of 1.25 fs was maintained and the simulation trajectory was created in every 1 ps.

The following equations were employed,

$$F(t) = \frac{1}{N}\sum_{i=1}^{N} F_i(t) \quad \text{..... eqn. (i)}$$

$$\int_0^{W_{dissc}} dw = \int_0^{x_{dissc}} g(x)dx$$

$$\text{Integrating, } W_{dissc} = \int_0^{x_{dissc}} g(x)dx \quad \text{..... eqn. (ii)}$$

Where,

W_{dissc} = Work done by the ligand until it's completely dissociated.

x_{dissc} = Distance at which occurs.

g(x) = Function of force subjected to the ligand concerning its dissociation.

2.4. Molecular dynamics simulations:

Both hACE2 and S-RBD protein with their respective screened molecules were subjected to molecular dynamics (MD) simulation studies to analyze the flexibility and stability of protein-ligand interactions[53]. The docked complexes were assessed based on interaction pattern, behavioural property, structural property, solvation property, fluctuation, conformational changes, and physical basis of function. The results of the different docked complexes were examined by using trajectory files. YASARA software was applied to

perform 100 ns of each MD system containing protein, ligand, and water molecules for protein-ligand complexes[54]. The total charge of the system was neutralized before the energy minimization and production by adding 0.9% NaCl at 298 K temperature and the AMBER14 force field was applied. The physiological pH was maintained at 7.4. The complex was energetically minimized using the step-down algorithm with 5000 steps after placing it in a cuboidal box. Afterward, to gain the long-range electrostatic interactions, the Particle Mesh Ewald (PME) summation was used. The systems were balanced by using the Berendsen thermostat and standard pressure (1.01325 bar) for 100 ps using the NPT (constant Number of particles, Pressure, and Temperature) to ensure the equal distribution of solvent and ions around the protein-ligand complexes. Finally, a 1.25 fs time step was used to carry out a period of 100 ns MD simulation[55]. The snapshots were saved at every 100 ps of the MD simulation for further analysis. Several other parameters such as RMSD (root mean square deviation), RMSF (root mean square fluctuation), and Rg (radius of gyration) were determined to explore the conformational changes and steadiness of the system.

Principal Component Analysis (PCA) was calculated from the last 90 ns of MD trajectory data. This technique is used to characterize structural quality change during MD comparing different drug-protein complexes. A screen plot was generated with the first component consisting of maximum possible information, then the second component that contains maximum remaining information, and so on. To pre-process data, an auto-scale function was used. R platform was used to calculate all calculations employing in-house developed codes. Plots were generated through the package ggplot2.

The following equation contains the important components of a PCA model,

$$X = T_K P_K^T + E$$

Where, X matrix is expressed as a product of two new matrices (i.e. T_K and P_K). T_K serves as the matrix of scores that represents how samples relate to each other, P_K represents the matrix of loadings that contain information about how variables relate to each other, k is the number of factors included in the model, and E is the matrix of residuals. Several other parameters such as RMSD (root mean square deviation), RMSF (root mean square fluctuation), and Rg (radius of gyration) were determined to explore the conformational changes and steadiness of the system.

2.5. Binding free energy calculation through MM-PBSA method:

The Molecular Mechanics-Poisson Boltzmann Surface Area (MM-PBSA) method was used to estimate the binding affinity of a ligand (molecules) in terms of binding free energy (ΔG_{bind}). YASARA dynamics was employed for all the calculations and AMBER14 force field was applied with the single trajectory approach[56]. Its significance in drug designing and macromolecular complex studies has already been proven[57,58]. It is a very effective method in finding inhibitors against protein targets. The ΔG_{bind} value for the selected snapshots from the 100 ns MD simulation is calculated for the top 3 selected ligands (molecules) for

both the targets (1R4L & 6M0J). The energy values related to protein (P), ligand (L), and protein-ligand complex (C) conformations were acquired from the MD trajectory using a single trajectory approach.

The ΔG_{bind} is obtained by the following equation,

$$\Delta G_{bind} = G_{complex} - G_{protein} - G_{ligand} \quad \text{..... eqn. (i)}$$

Where,

$G_{complex}$ = Total free energy of the complex between protein and ligand

$G_{protein}$ = Free energy of the protein in the solvent

G_{ligand} = Free energy of the ligand in the solvent

The free energy of any individual component (complex, protein, and ligand) given by,

$$\Delta G_{bind} = \Delta G_{MM} + \Delta G_{PB} + \Delta G_{SA-T\Delta S} \quad \text{..... eqn. (ii)}$$

Where,

ΔG_{MM} = Average molecular mechanics (MM) potential energy in a vacuum

ΔG_{PB} = Polar solvation energy

ΔG_{SA} = Non-polar solvation energy

$T\Delta S$ = Contribution of entropy to the free energy (T= Temperature and S= Entropy)

G_{MM} has two terms and is defined as,

$$G_{MM} = G_{bonded} + G_{nonbonded} \text{..... eqn. (iii)}$$

$$G_{MM} = G_{bonded} + G_{elec} + G_{vdW} \text{..... eqn. (iv)}$$

Where,

G_{bonded} = Bonded interactions included bond-length, bond-angle, and dihedral angle

$G_{non\text{-}bonded}$ = Non-bonding interactions included electrostatic and van der Waals interaction

The $G_{solvation}$ = Energy needed to move a solute from a vacuum to the solvent. It can be expressed as,

$$G_{solvation} = G_{polar} + G_{nonpolar} \text{..... eqn. (v)}$$

2.6. In-silico pharmacokinetics, drug-likeliness, and ADMET profile analysis:

The pharmacological significance of the following selected ligands (phyto-compounds) for both the targets (1R4L & 6M0J) was conducted by the online free available web tool (i.e. admetSAR/SwissADME)[59,60]. The desired parameters were selected to analyze physicochemical, pharmacokinetic, drug likeliness, water-solubility, phytochemical-like properties, Lipinski's rule of five (LoF), Veber's rule, and ADMET. For finding a suitable drug candidate, pharmacokinetics (i.e. fate of substance) and pharmacodynamics (i.e.

effects and mechanism) research must be conducted[61,62]. The LoF rule is used to elucidate drug likeliness whereas; the flexibility and the surface area of any suitable molecules are evaluated by Veber's rule. ADMET plays a crucial role in developing desired drug candidates. A high-quality drug candidate should always possess sufficient efficacy as well as appropriate ADMET properties against the therapeutic target. The ADMET score is determined by the three parameters: (i) the accuracy rate of the model, (ii) the importance of the endpoint in the process of pharmacokinetics, and (iii) the usefulness index.

The ADMET score is calculated as,

$$\text{ADMET score} = \frac{\sum_{i=1}^{n} w_i \times q}{\sum_{i=1}^{n} w_i}$$

Where,

q = the transformed result [beneficial/positive, q= 1 and harmful/negative, q= 0].

w_i = the weight applied to each endpoint.

n = the number of endpoints.

All the top 5 desired phytochemicals for both the targets (1R4L & 6M0J) were examined for drug likeliness/pharmacophore features obeying Lipinski's rule of five (LoF) based on physicochemical properties upon submission of Simplified Molecular Input Line Entry System (SMILES) format as an input of respective chemical entities such as Molecular Weight (g/mol), AlogP, H-bond Acceptor, H-bond Donor, Water Solubility (LogS). Thereafter, The ADMET properties such as Human Intestinal Absorption, Blood-Brain Barrier, Caco-2 permeability, Ames Mutagenesis are important parameters for the selection of the appropriate drug-like compounds by employing an online free webserver (i.e. admetSAR). Thus, the following attributes are very important during drug development processes for any phytochemical entities[63,64].

3. Results

3.1. Virtual screening:

In this research, structure-based virtual screening (SBVS) was carried out in which 3D structures of the biological target were obtained from the X-ray, NMR, or computational modeling, which aims to understand the molecular interactions involved in ligand-protein binding and thus, interpret experimental results. The VSW tool is projected to run an entire sequence of jobs for screening large collections of phyto-compounds (1000 phytomolecules) against hACE2 and spike RBD of SARS CoV-2. The tool is unified with the subsequent multi-step molecular docking that includes Glide-HTVS (High-Throughput Virtual Screening), Glide-SP (Standard Precision,) and Glide-XP (Xtra Precision) and finally, the estimation of binding free energy using the MM-PBSA approach followed by drug likeliness and ADMET profile analysis.

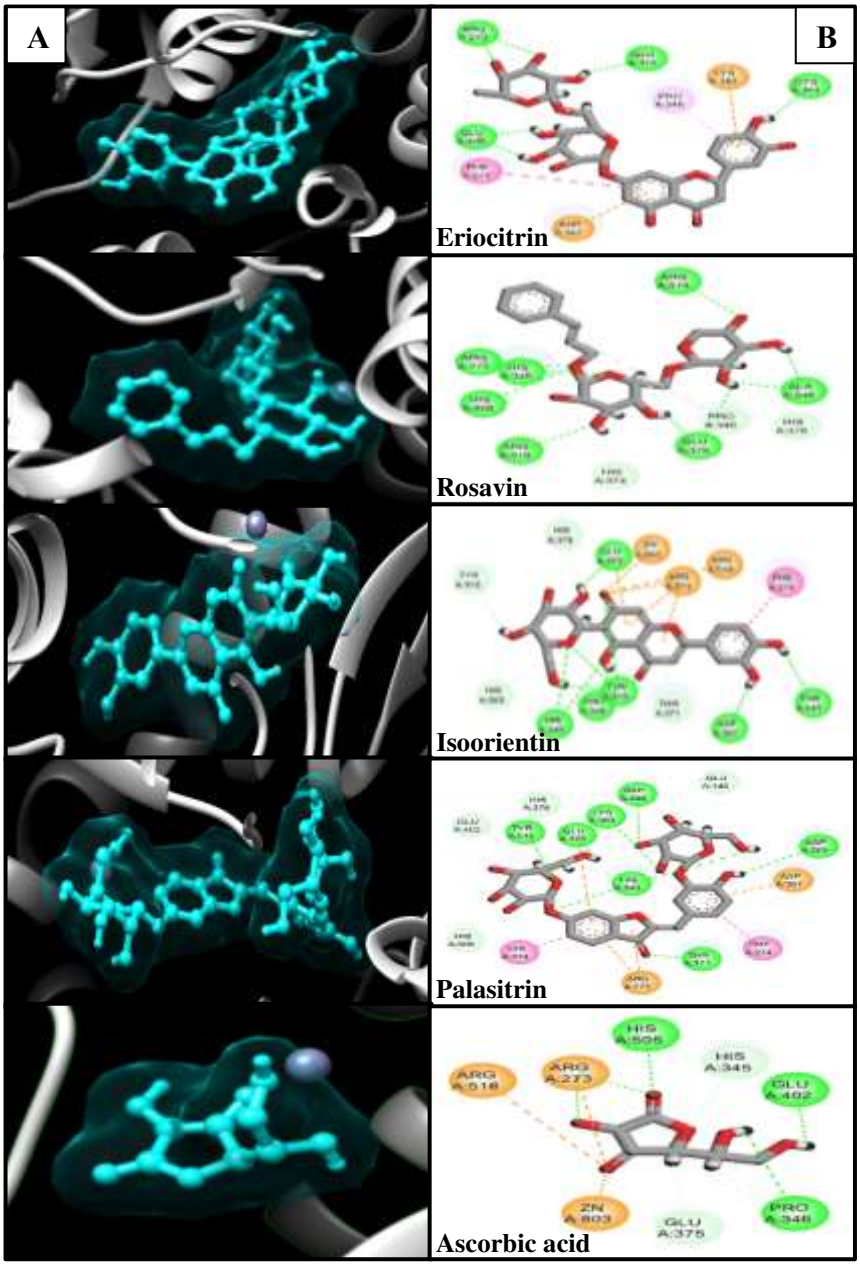
A
B
Eriocitrin
Rosavin
Isoorientin
Palasitrin
HIS A:505
HIS A:345
ARG A:518
ARG A:273
GLU A:402
ZN A:803
GLU A:375
PRO A:346
Ascorbic acid

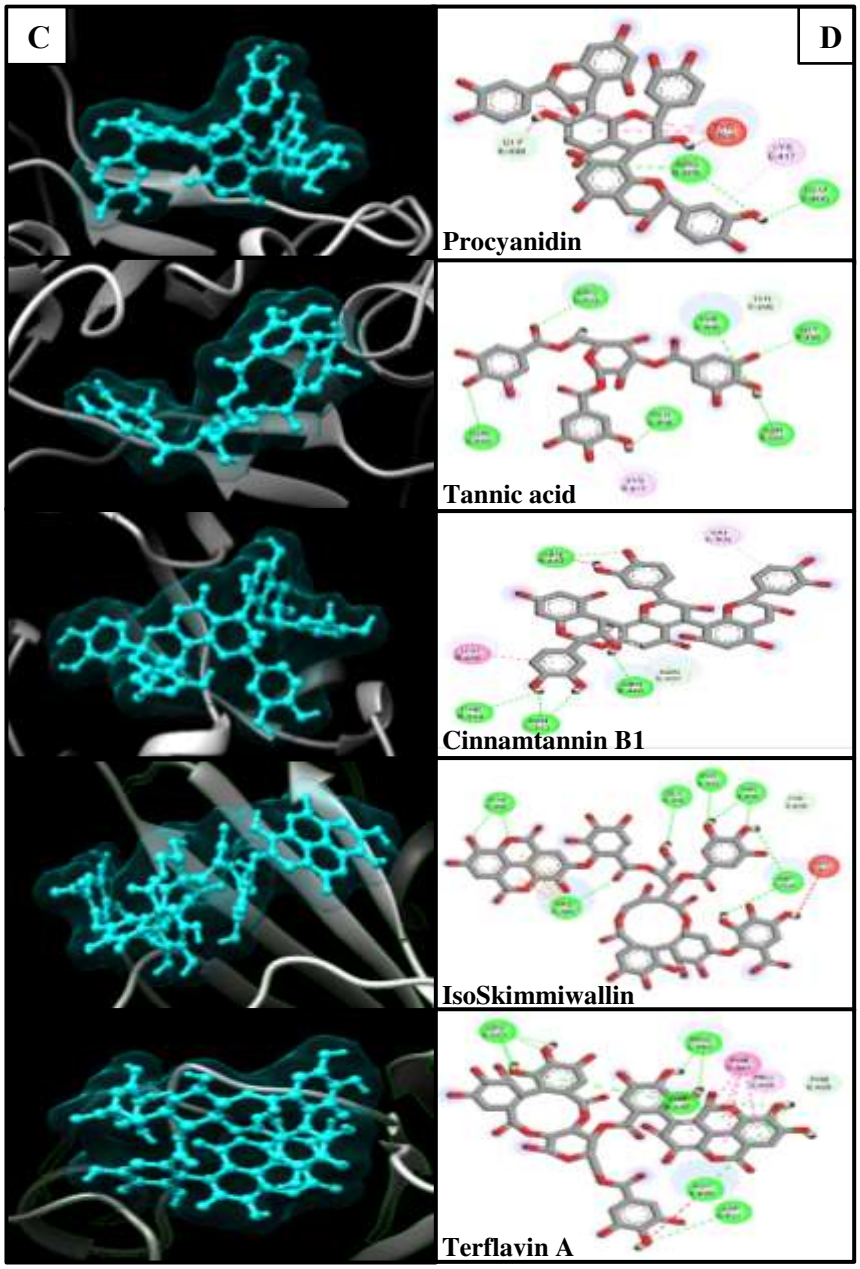

Figure 1: Molecular interaction analysis of screening hit within the binding cavity of hACE2 and S-RBD protein. (A&C) 3D representation of the protein target surface structure with interacting ligands (1R4L: Eriocitrin to Ascorbic acid and 6M0J: Procyanidin to Terflavin A) present in binding pocket shown in ball and stick representation in cyan color. (B&D) 2D representation, a ligand is shown in the red-grey line model while the interacting residues are shown in discs. Dark green lines represent conventional H-bond, Light green lines represent a carbon-hydrogen bond, Dark pink lines represent pi-pi stacked, Light pink lines represent a pi-alkyl bond, Dark orange lines represent pi-cation/pi-anion/attractive charge, and Dark red lines represent unfavorable donor-donor interactions.

3.2. Molecular docking analysis:

Molecular docking is a versatile method used to study the interaction between small molecules and a protein at the atomic level. Therein, predicting the binding efficiency, and the types of protein-ligand interactions between them. After defining the grid box *via* the Receptor Grid Generation tool of Glide in Maestro, the X-ray crystal structure of the human ACE2 (1R4L) and spike-RBD domain of SARS-CoV-2 (6M0J) are used for the identification of plant-based bioactive compounds as a potential inhibitor binding against viral protein. The best-docked pose of each molecule was initially selected by considering the lowest XP-dock score among all the generated poses. These scores represent the top 5 best-bound ligand conformations and relative binding affinities for both targets. **Table 1** consists of all the compounds with their drug name & PubChem ID, docking scores, MM-PBSA, and necessary H-bond formation with possible active residues by ligands with targets required for the inhibition of receptor of SARS-CoV-2. The compound with the least binding energy is regarded as the best mode of binding (higher docking scores) as it is most stable for the ligand. The docking score for both the targets; (1R4L: Eriocitrin, Rosavin, Isoorientin, Palasitrin, and Ascorbic Acid) & (6M0J: Procyanidin C1, Tannic Acid, Cinnamtannin B1, Isoskimmiwallin and Terflavin A) was found to be -11.045, -9.01, -11.982, -11.366 and -11.47 kcal/mol & -10.582, -6.606, -7.752, -8.51 and -8.29 kcal/mol respectively. The detailed molecular interaction analysis of these phytochemical compounds at the active site of hACE2 and S-RBD domain of SARS-CoV-2 revealed that most of the interactions are within the reported active site amino acid residues as represented in **figure 1**.Interestingly, a few amino acids (active site residues) were found to establish the salt bridges with compounds. The salt bridge interaction is formed between two groups of opposite charge and plays an important role to form the stable protein-ligand complex. This compound exhibits several medicinal properties including anti-proliferative and anti-viral activities. All these screened lead molecules showed lower and significant binding energy and novel hydrogen bonding interactions with active site residues of target receptors along with electrostatic and hydrophobic interactions. **Table 2** consists of inhibition constant (pKi), and ligand efficiency (LE). Ligand efficiency is the negative ratio of the docking binding energy in kcal/mol to the number of heavy atoms. The inhibition constant (pKi) value for both the targets (1R4L: Eriocitrin, Rosavin, Isoorientin, Palasitrin, and Ascorbic Acid) & (6M0J: Procyanidin C1, Tannic Acid, Cinnamtannin B1, Isoskimmiwallin and Terflavin A) was found to be 8.09604, 6.604375, 8.782866, 8.331335, and 8.407568 & 7.756659, 4.842231, 5.682255, 6.237873, and 6.076612 respectively. The ligand efficiency (LE) was found to be 0.262976, 0.300333, 0.374438, 0.270619, and 0.955833 & 0.167968, 0.1468, 0.123048, 0.094556, and 0.106282 respectively. All the molecules were found to have LE value of less than 0.6 which indicates the potentiality and drug-likeness of the compounds. Thus, the above crucial observation about diverse binding interactions between the proposed molecules and ligand-binding amino residues along with pKi and LE undoubtedly explained the inhibitory potential of selected lead molecules against targeted protein.

Table 1: Phytochemicals depicting binding energy score and interacting residue with hACE2 and S-RBD protein target.

Protein	Drug Name & PubChem ID	Molecular Docking Score (kcal/mol)	Types of Interacting Amino acid	Distance	Bond Category	Bond Type
1R4L	Eriocitrin (83489)	-11.045	Arg273	1.79547	H-bond	Conventional H-bond
				2.34704	H-bond	Conventional H-bond
				2.14884	H-bond	Conventional H-bond
			Glu406	1.71446	H-bond	Conventional H-bond
				2.26539	H-bond	Conventional H-bond
				2.31988	H-bond	Carbon H-bond
				2.73191	H-bond	Carbon H-bond
			Glu375	2.27195	H-bond	Conventional H-bond
				2.83543	H-bond	Carbon H-bond
			Phe274	4.62331	Hydrophobic	Pi-Pi Stacked
			Asp367	3.53166	Electrostatic	Pi-Anion
			Pro346	4.35191	Hydrophobic	Pi-Alkyl
			Lys363	4.75221	Electrostatic	Pi-Cation
			Cys344	1.9863	H-bond	Conventional H-bond
	Rosavin (9823887)	-9.01	Ala348	1.93894	H-bond	Conventional H-bond
				2.42473	H-bond	Conventional H-bond
			His378	2.66195	H-bond	Carbon H-bond
			Pro346	2.64171	H-bond	Carbon H-bond
				5.28218	Hydrophobic	Alkyl
			Glu375	1.81061	H-bond	Conventional H-bond
				2.346	H-bond	Conventional H-bond
				3.01988	H-bond	Carbon H-bond
				3.04134	H-bond	Carbon H-bond
			His374	2.30935	H-bond	Pi-Donor H-bond
			Arg518	2.83549	H-bond	Conventional H-bond
			His505	2.63316	H-bond	Conventional H-bond
				2.96326	H-bond	Carbon H-bond
			His345	1.70953	H-bond	Conventional H-bond
				3.77089	Hydrophobic	Pi-Alkyl
			Arg273	1.9337	H-bond	Conventional H-bond
			Arg514	2.63953	H-bond	Conventional H-bond

				2.54772	H-bond	Conventional H-bond
	Isoorientin (114776)	-11.982	Arg273	5.1942 4.70644 4.96818	Electrostatic Electrostatic Electrostatic	Attractive Charge Pi-Cation Pi-Cation
			Arg518	5.09779	Electrostatic	Attractive Charge
			Zn803	2.04046	Electrostatic	Attractive Charge
			Glu375	3.63114 1.93508	Electrostatic H-bond	Pi-Anion Conventional H-bond
			His378	2.55723	H-bond	Carbon H-bond
			Tyr510	2.61797	H-bond	Pi-Donor H-bond
			His505	2.8399	H-bond	Carbon H-bond
			His345	2.73531 2.69571	H-bond H-bond	Conventional H-bond Conventional H-bond
			Pro346	1.97731 2.87789 2.27502	H-bond H-bond H-bond	Conventional H-bond Carbon H-bond Carbon H-bond
			Tyr515	2.89743 2.45466 1.86495	H-bond H-bond H-bond	Conventional H-bond Conventional H-bond Conventional H-bond
			Thr371	3.04963	H-bond	Pi-Donor H-bond
			Asp367	1.88077	H-bond	Conventional H-bond

			Thr445	2.67469	H-bond	Conventional H-bond
			Phe274	4.83427	Hydrophobic	Pi-Pi Stacked
	Palasitrin (42607742)	-11.366	His345	2.13854 2.19806	H-bond H-bond	Conventional H-bond Conventional H-bond
			Lys363	2.20373	H-bond	Conventional H-bond
			Asp368	2.69335	H-bond	Conventional H-bond
			Thr371	2.07035	H-bond	Conventional H-bond
			Tyr515	1.97202	H-bond	Conventional H-bond
			Glu375	1.8082 3.05707 4.19576	H-bond H-bond Electrostatic	Conventional H-bond Carbon H-bond Pi-Anion
			Asp269	3.05665	H-bond	Conventional H-bond
			His505	2.41759	H-bond	Carbon H-bond
			Glu145	2.45954 2.83381	H-bond H-bond	Carbon H-bond Carbon H-bond
			His378	2.91255	H-bond	Carbon H-bond

			Glu402	2.54921	H-bond	Carbon H-bond
			Arg273	4.28175	Electrostatic	Pi-Cation
				4.74396	Electrostatic	Pi-Cation
			Asp367	4.24232	Electrostatic	Pi-Anion
			Phe274	5.08459	Hydrophobic	Pi-Pi Stacked
			His374	5.1058	Hydrophobic	Pi-Pi T-shaped
	Ascorbic acid (54670067)	-11.47	Arg273	5.36944	Electrostatic	Attractive Charge
				1.64187	H-bond	Conventional H-bond
				1.67866	H-bond	Conventional H-bond
			Arg518	4.85589	Electrostatic	Attractive Charge
			Zn803	1.97523	Electrostatic	Attractive Charge
			His505	2.12228	H-bond	Conventional H-bond
			Pro346	2.81539	H-bond	Conventional H-bond
				2.88617	H-bond	Carbon H-bond
				2.48569	H-bond	Carbon H-bond
			Glu402	2.3643	H-bond	Conventional H-bond
			His345	3.08042	H-bond	Carbon H-bond
			Glu375	2.25978	H-bond	Carbon H-bond
6M0J	Procyanidin C1 (169853)	-10.582	Glu406	2.15221	H-bond	Conventional H-bond
			Arg403	1.95889	H-bond	Conventional H-bond
				2.63767	H-bond	Conventional H-bond
			Gly496	2.80793	H-bond	Carbon H-bond
			Tyr505	5.15484	Hydrophobic	Pi-Pi T-shaped
				5.29035	Hydrophobic	Pi-Pi T-shaped
			Lys417	5.39073	Hydrophobic	Pi-Alkyl
	Tannic Acid (250395)	-6.606	Glu406	2.46847	H-bond	Conventional H-bond
			Asn501	2.33709	H-bond	Conventional H-bond
			Tyr505	2.39569	H-bond	Conventional H-bond
				2.93081	H-bond	Carbon H-bond
			Arg403	2.10667	H-bond	Conventional H-bond
			Gln409	2.86627	H-bond	Conventional H-bond
			Gly496	2.28843	H-bond	Conventional H-bond
			Tyr495	2.85535	H-bond	Carbon H-bond

			Lys417	3.85561	Hydrophobic	Pi-Alkyl
	Cinnamtannin B1 (475277)	-7.752	Asn440	2.58573	H-bond	Conventional H-bond
			Asn343	2.31762	H-bond	Conventional H-bond
				2.15154	H-bond	Conventional H-bond
			Phe342	2.73249	H-bond	Conventional H-bond
			Asn439	1.99388	H-bond	Conventional H-bond
			Asn437	2.75323	H-bond	Carbon H-bond
			Trp436	4.80565	Hydrophobic	Pi-Pi Stacked
				3.83523	Hydrophobic	Pi-Pi Stacked
			Val503	4.96046	Hydrophobic	Pi-Alkyl
	IsoSkimmiwallin (16130370)	-8.51	Thr430	2.25039	H-bond	Conventional H-bond
				2.10117	H-bond	Conventional H-bond
			Asp428	2.76409	H-bond	Conventional H-bond
				2.45155	H-bond	Conventional H-bond
			Glu516	3.01965	H-bond	Conventional H-bond
			Arg355	1.76659	H-bond	Conventional H-bond
				4.31638	Electrostatic	Pi-Cation
				4.53109	Electrostatic	Pi-Cation
				4.15049	Electrostatic	Pi-Cation
				5.10956	Hydrophobic	Pi-Alkyl
				5.04767	Hydrophobic	Pi-Alkyl
				3.82626	Hydrophobic	Pi-Alkyl
			Arg466	1.9183	H-bond	Conventional H-bond
				2.2776	H-bond	Conventional H-bond
			Phe515	2.4858	H-bond	Conventional H-bond
			Phe429	2.70532	H-bond	Carbon H-bond
	Terflavin A (16175788)	-8.29	Leu517	2.30448	H-bond	Conventional H-bond
				2.12891	H-bond	Conventional H-bond
				1.84946	H-bond	Conventional H-bond
				2.69445	H-bond	Conventional H-bond

			Pro463	2.32459	H-bond	Conventional H-bond
				2.31066	H-bond	Conventional H-bond
				4.98047	Hydrophobic	Pi-Alkyl
			Asp428	2.31315	H-bond	Conventional H-bond
			Thr430	1.99042	H-bond	Conventional H-bond
				2.42405	H-bond	Conventional H-bond
				2.44632	H-bond	Conventional H-bond
			Asp427	2.39579	H-bond	Conventional H-bond
			Phe429	1.69151	H-bond	Carbon H-bond
			Phe464	4.92971	Hydrophobic	Pi-Pi T-shaped
				5.05818	Hydrophobic	Pi-Pi T-shaped
				5.41727	Hydrophobic	Pi-Pi T-shaped
				4.97067	Hydrophobic	Pi-Pi T-shaped
			Pro426	4.69061	Hydrophobic	Pi-Alkyl
				5.44062	Hydrophobic	Pi-Alkyl

Table 2: Inhibition constant (pKi) and ligand efficiency (LE) value of top five ligands against hACE2 and S-RBD receptors.

Protein	Drug	Inhibition constant (pKi)	Ligand efficiency (LE)
1R4L	Eriocitrin	8.09604	0.262976
	Rosavin	6.604375	0.300333
	Isoorientin	8.782866	0.374438
	Palasitrin	8.331335	0.270619
	Ascorbic acid	8.407568	0.955833
6M0J	Procyanidin C1	7.756659	0.167968
	Tannic acid	4.842231	0.1468
	Cinnamtannin B1	5.682255	0.123048
	IsoSkimmiwallin	6.237873	0.094556
	Terflavin A	6.076612	0.106282

3.3. Steered molecular dynamics (SMD) analysis:

To investigate the binding properties of top 5 selected ligands-proteins complex, the Steered Molecular Dynamic (SMD) simulation was performed. The average force was calculated from the 3 independent runs of each protein-ligand complex during the unbinding process and F_{max} (maximum force obtained from the average values) was recorded in **Table 3**. In addition, work from every simulation was calculated and then, W_{max} was noted from the average values for each complex (**Table 3**). The greater force and work value indicate strong binding of ligands with their respective proteins.

Table 3: The obtained maximum force and work done by 5 potent drugs for both the targets (1R4L & 6M0J) against their respective proteins during SMD simulation.

Protein	Drug	F_{max} (pN)	W_{max} (kcal/mol)
ACE2	Eriocitrin	4804.309	1294.042
	Rosavin	6082.755	1240.697
	Isoorientin	6871.666	1994.970
	Palasitrin	4738.713	1374.663
	Ascorbic acid	3358.786	771.259
RBD	Procyanidin C1	1151.463	172.734
	Tannic acid	1551.828	50.996
	Cinnamtannin B1	1794.978	191.658
	IsoSkimmiwallin	1665.646	337.248
	Terflavin A	1443.669	249.389

Isoorientin exhibits the best performance where it asserts the highest force value of 6871.666 pN and the highest internal work value of 1994.970 kcal/mol compared to other 4 drugs against Angiotensin-Converting Enzyme 2 (ACE2) protein. Rosavin denotes the second-highest force (6082.755 pN) whereas Palasitrin displays the second highest work (1374.663 kcal/mol) against ACE2 receptor protein. Based on the maximum force and work values Isoorientin, Rosavin, and Palasitrin could be potent inhibitors against ACE2 receptor protein. The other two ligands (Eriocitrin and Ascorbic acid) manifest a lower value of force (4804.309 pN, 3358.786 pN) and work (1294.042 kcal/mol, 771.259 kcal/mol) than the previously discussed ligands. In the cases of spike receptor-binding domain (RBD) protein, the second-highest force value of 1665.646 pN and the highest work value of 337.248 kcal/mol were observed for IsoSkimmiwallin, suggesting that IsoSkimmiwallin might be an active ligand with great inhibition efficacy. Cinnamtannin depicts the highest force (1794.978 pN) whereas Terflavin A maintains the second-highest work (249.389 kcal/mol) done internally. It can be summarized that Cinnamtannin, IsoSkimmiwallin, and Terflavin A ligands are strongly bound to the RBD protein in comparison with Procyanidin C1 and Tannic acid.

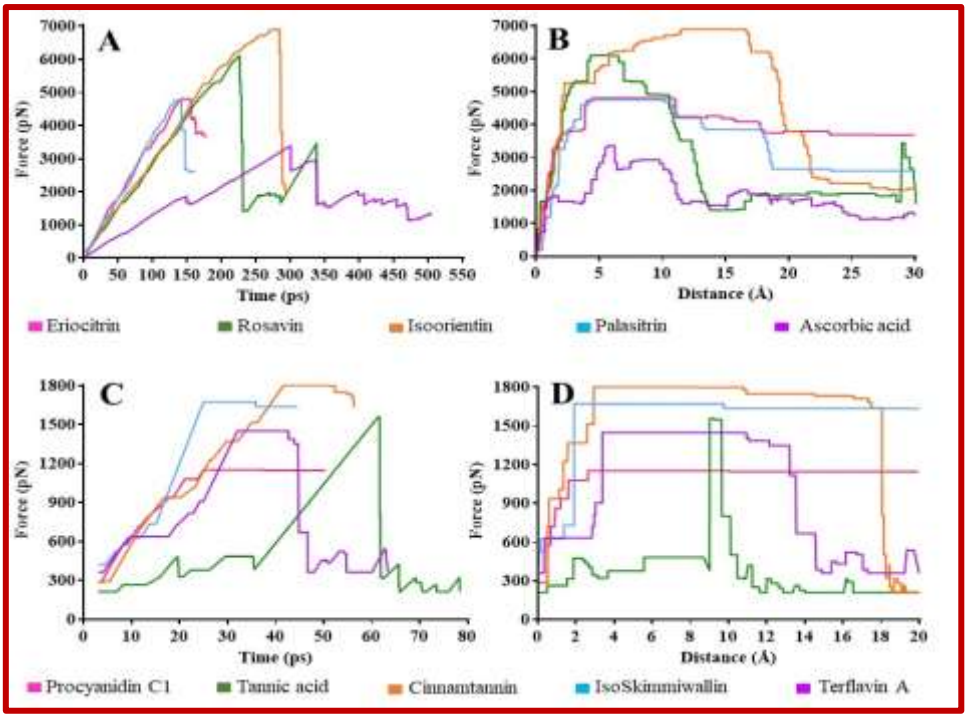

Figure 2: Steered Molecular Dynamic (SMD) simulations of 10 ligands (1R4L & 6M0J). **(A) & (B)** Force vs. Time graph and Force vs. Distance graph, respectively; against ACE2 receptor protein and **(C) & (D)** Force vs. Time graph and Force vs. Distance graph, respectively; against RBD protein.

In **Figure 2**, the graphical representation of pulling force at various time points (**A** and **C**) and in terms of the distance (**B** and **D**) between the centre of mass of the protein cavity and the ligand is demonstrated. Generally, the force is increasing concerning the time and distance and when it reaches rupture force, the force value is falling gradually **Figure 2(A)**. Steered Molecular Dynamic simulation runs not only throughout the complete dissociation period of the bound ligand but until the time needed to reach the system at the defined distance. In ACE2 receptor protein, the rupture force of Isoorientin and the rupture force of Rosavin were remarked around 270 ps and 224 ps, respectively. Though the applied force of Rosavin decreases slowly after the complete detachment, the force is increased suddenly after 235 ps. Sometimes, the force is still increasing by a small portion, in due time after the ligand has no any kind of nonbinding interaction with protein because of friction solvation. However, this kind of force increase is small and can be ignored. Eriocitrin and Palasitrin completed their simulation within 178 ps and 162ps, respectively, claiming their rupture forces around 141 ps and 131 ps, respectively. On contrary, Ascorbic acid illustrates the lowest rupture force at 298 ps compared to the other four ligands. The force vs. Distance graph for ACE2 receptor protein **Figure 2(B)** also displays the same manner graph as **Figure 2(A).**

Figures 2(C) and 2(D) reveal that forces of all ligands are increasing and remain constant at the rupture force, except Tannic acid. Though the rupture force is falling after the detachment of Cinnamtannin, Tannic acid, IsoSkimmiwallin, and Terflavin A, it remains constant till the end of the simulation for Procyanidin C1. However, Procyanidin C1, Tannic acid, Cinnamtannin, IsoSkimmiwallin, and Terflavin A are exhibiting their rupture forces at 25 ps, 61 ps, 49 ps, 32 ps, and 38 ps, respectively **Figure 2(C)**. The force vs. Distance

graph for RBD also manifests the same manner graph like the Force vs. Time graph where forces of all ligands are increasing like a zigzag pattern concerning distances.

The SMD results show Isoorientin, Rosavin, and Palasitrin ligands for ACE2 receptor protein and Cinnamtannin, IsoSkimmiwallin, and Terflavin A ligands for RBD protein might be efficient candidates to impede the Covid19 catastrophe. These ligands are chosen for Molecular Dynamic Simulation. Structural representation of our 6 best drugs against their correspondent proteins in SMD is illustrated in **Figure 3** and **Figure 4**.

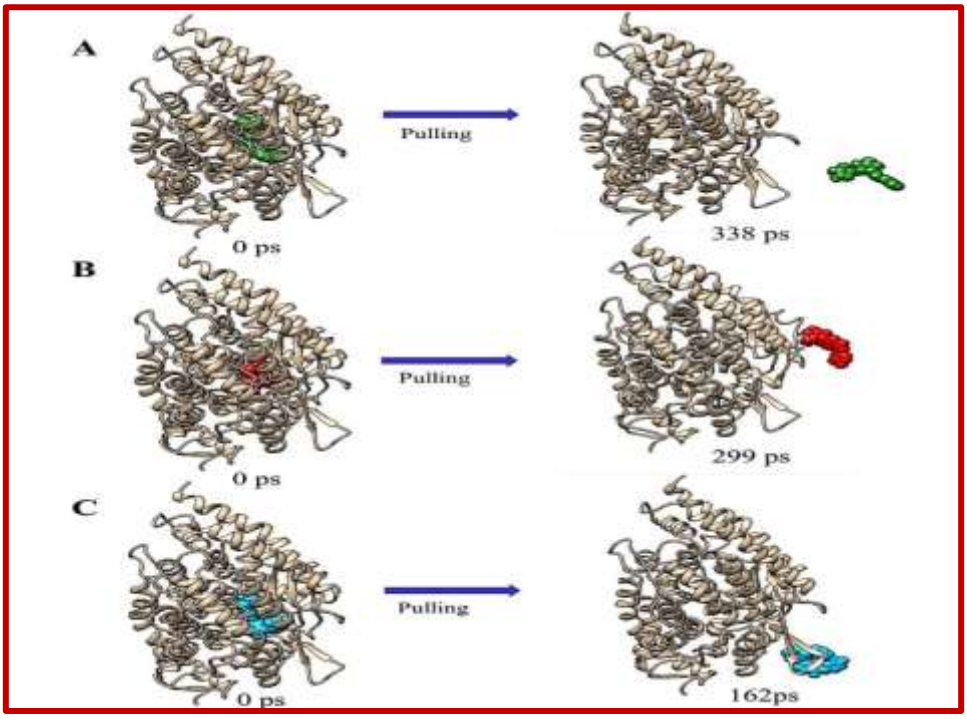

Figure 3: Structural representations of 3 best ligands against ACE2 receptor protein in Steered Molecular Dynamic simulations before and after dissociation. A) Rosavin-ACE2 complex (Rosavin- deep green, ACE2- tan); B) Isoorientin-ACE2 complex (Isoorientin- red); C) Palasitrin-ACE2 complex (Palasitrin- sky blue).

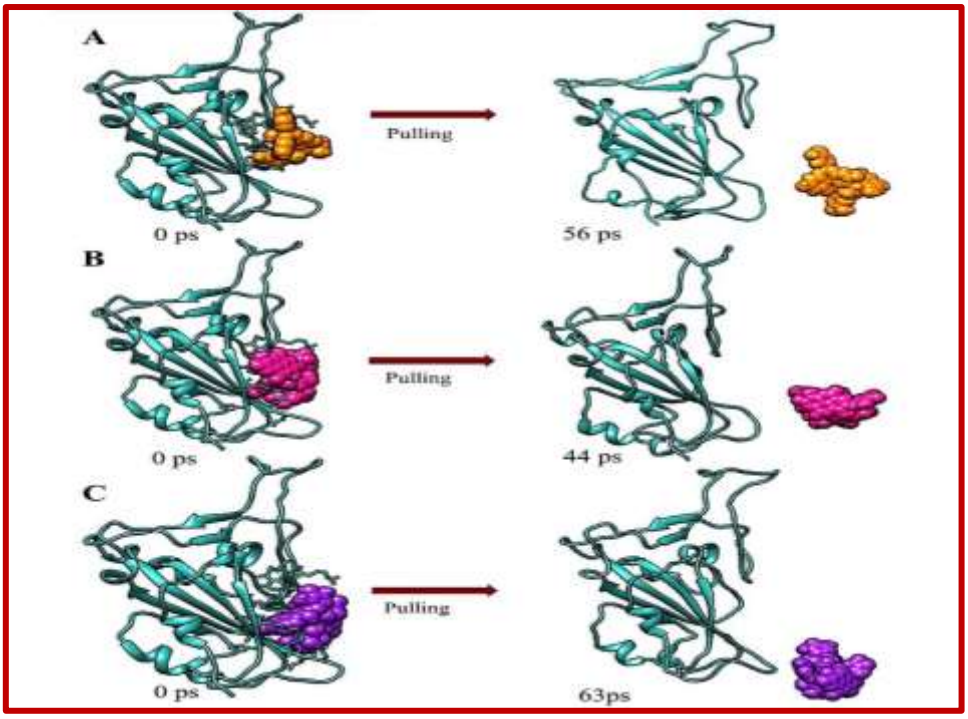

Figure 4: Structural representations of 3 best ligands against RBD protein in Steered Molecular Dynamic simulations before and after dissociation. A) Cinnamtannin-ACE2 complex (Cinnamtannin- orange, RBD- sea green); B) IsoSkimmiwallin-ACE2 complex (IsoSkimmiwallin- pink); C) Terflavin A-ACE2 complex (Terflavin A- violet).

3.4. Molecular dynamics simulations:

The interaction and stability of drug molecules with proteins is investigated *via* molecular dynamic simulation in order to get insight in to behavioral and dynamical characteristics of the protein-ligand complex. The resulting changes in protein structure and function may impact many aspects of drug discovery, drug development, and drug action. In **Figures 5 and 6**, we examined the structural stability of three drug-protein complexes by calculating several structural order parameters. An all-atoms MD simulation of each docked complex of proposed molecules was explored for a 100ns time span. Several parameters such as RMSD, Rg, SASA, and RMSF were obtained from the MD simulation trajectory. Each of the above parameters explains the stability of the protein-ligand complex in the dynamics states. The entire trajectory was further used for the calculation of binding free energy through the MM-PBSA approach.

3.4.1. Root-mean-square deviation (RMSD):

The protein backbone RMSD received from the simulation trajectory of the protein-ligand complex explains the steadiness of the complex in the dynamic surroundings. The higher protein-backbone RMSD value indicates unfolding and contrarily the lower value favours the compactness. The low fluctuation of the backbone RMSD also validates the equilibration of the protein-ligand complex. The difference between the maximum and minimum RMSD confer a concept about the backbone deviation. The lower RMSD value of

each complex undoubtedly defined the stableness and consistency of the complexes inside the dynamic environment and is considered one of the crucial parameters according to Shukla and Tripathi, 2020[65]. RMSD plot of both the complexes (Apo, 1R4L: Rosavin-blue line, Isoorientin-green line, Palasitrin-yellow line) and (Apo, 6M0J: Cinnamtannin-blue line, IsoSkimmiwallin-yellow line & Terflavin A-green line) exhibited instant deviation from 0 Å to 1.2 Å and are observed getting stabilized at the end of the simulation deviated in the range of 1.4-1.9 Å (1R4L) and 1.0-1.5 Å (6M0J) suggesting protein stability after binding of the ligand. Though, a lot of steep peaks can be seen during the simulation which is a result of the internal vibration of the molecule.

The RMSD value is calculated with respect to the reference native conformation r_{ref} using the following formula:

$$\mathrm{RMSD(t)} = \left[\frac{1}{M}\sum_{i=1}^{N} m_i \left| r_i(t) - r_i^{ref} \right|^2\right]^{1/2}$$

3.4.2. Radius of Gyration (Rg):

The Rg is one of the vital frameworks derived from the MD simulation trajectory to test the firmness of the protein-ligand complexes. It is linked with the tertiary structure and general conformational state defining our understanding of compactness and folding of the protein. Less deviation and steady variation of the Rg explain the steady folding of protein during the implementation of MD simulation. All three complexes of both targets were allowed to yield the Rg plot. The protein complexes along with ligands are observed with no abnormal or unusual deviation. A slight deviation was seen in protein-ligand complexes to some extent and afterward the system achieved stability that suggests the compactness of the system. This sudden deviation might be due to protein's packing. A fluctuation of 24.2-24.6 Å and 18.2-18.6 Å around the average values were observed for (ACE2: Rosavin-blue line, Isoorientin-green line & Palasitrin-yellow line) and (RBD: Cinnamtannin-blue line, IsoSkimmiwallin-yellow line & Terflavin A-green line) respectively. The difference between the highest and lowest Rg value illustrates an idea about the deviation of each system. All three plots attained the equilibrium around their average value thus, determining the compactness of the protein-ligand complexes throughout the simulation course.

3.4.3. Solvent accessible surface areas (SASA):

SASA was calculated to monitor the possible changes in the solvation environment upon ligand binding. It has always been considered a decisive factor in protein folding and stability studies. The average value of SASA observed were: 350 $Å^2$, 450 $Å^2$ & 400 $Å^2$ and 250 $Å^2$, 300 $Å^2$ & 250 $Å^2$ respectively for (ACE2: Rosavin-blue line, Isoorientin-green line & Palasitrin-yellow line) and (RBD: Cinnamtannin-blue line, IsoSkimmiwallin-yellow line & Terflavin A-green line). Generally, the increased value of the protein SASA

during simulation indicates structural relaxations. It means larger surfaces are in contact with water molecules (i.e. more number of inner residues coming in contact with the solvent) and therefore reduced protein stabilities. Lower SASA values suggest complexes are more stable with fewer inner residues interacting with surroundings. Although, the attained equilibrium throughout the simulation in each case suggests that the complexes are structurally stable.

3.4.4. Root-mean-square fluctuation (RMSF):

Each amino acid residue belonging to the protein-ligand complex is accountable for the stability of the dynamic processes. The fluctuation of any specific amino acid concerning the reference or native structure can be measured through the RMSF parameter calculated from the MD simulation trajectories. RMSF plot helped in understanding the residual vibrations in three different complexes. Since the alpha helixes and beta strands are rigid and well organized. Hence, less fluctuation is observed with the residues involved in such secondary structures. Whereas, loosely structures like bends and coils showed large RMSF value which indicates the instability or else the residue remains stable. The RMSF of each amino residue of all three complexes was calculated from the MD simulation trajectories. Amino acid residues of both the target were seen to fluctuate in an almost similar manner throughout the simulation. With a few exemptions, a slight fluctuation was observed which favours the stability of the amino residues in a dynamic state. Such observation might be due to conformation changes of amino acids to accommodate the ligand in the receptor cavity.

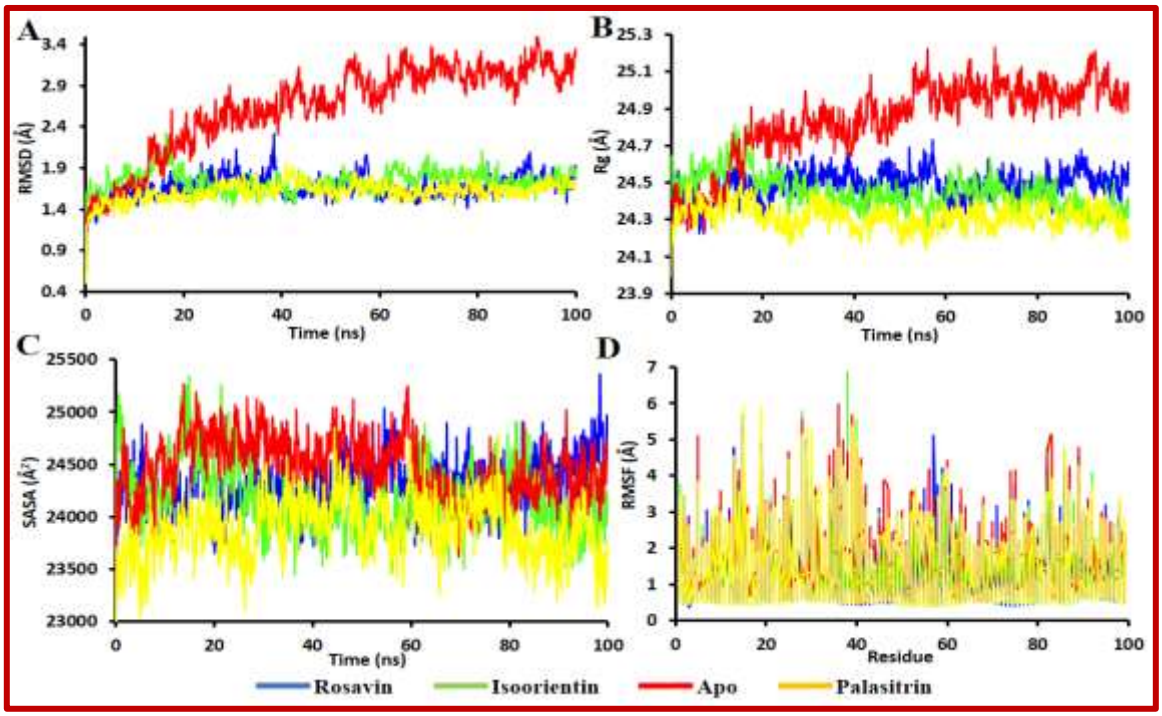

Figure 5: Molecular dynamics simulation (A) Root-mean-square deviation (RMSD), (B) Radius of gyration (Rg), (C) Solvent accessible surface area (SASA), and (D) Root mean square fluctuation (RMSF) of SARS-CoV-2 hACE2 (PDB ID: 1R4L).

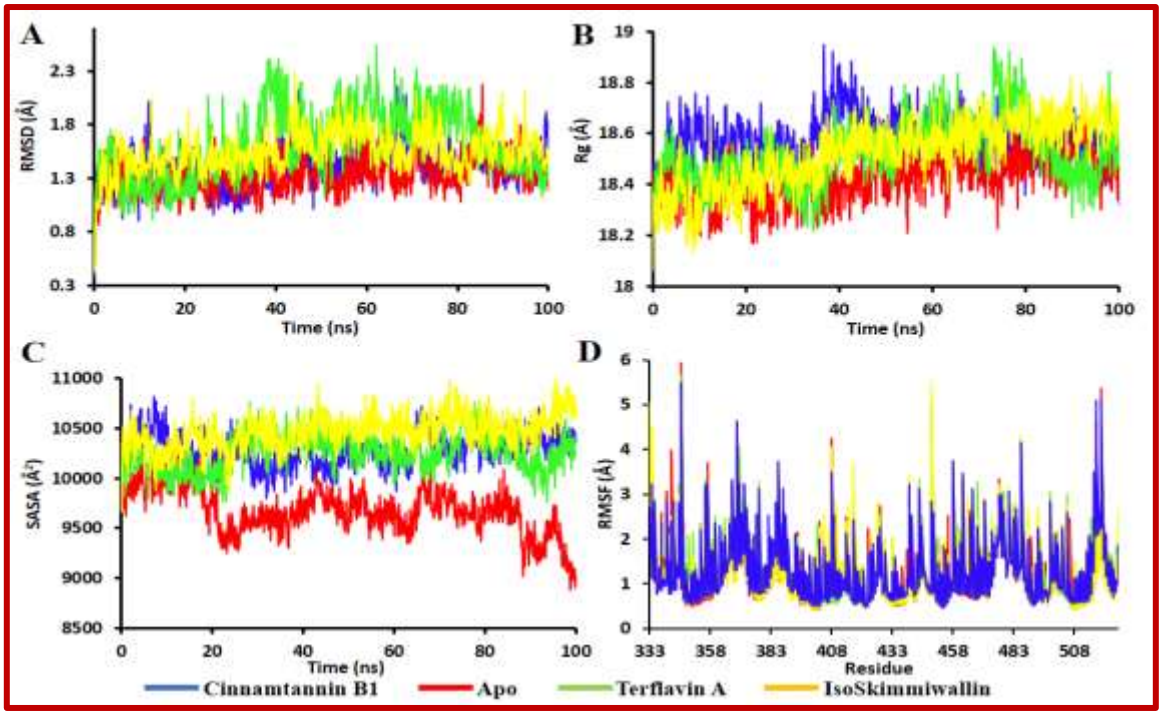

Figure 6: Molecular dynamics simulation (A) Root-mean-square deviation (RMSD), (B) Radius of gyration (Rg), (C) Solvent accessible surface area (SASA), and (D) Root mean square fluctuation (RMSF) of SARS-CoV-2 spike-RBD (PDB ID: 6M0J).

3.5. Principal Component Analysis:

PCA model for the structural and energy changes in case of both protein-apo and protein-ligands is generated over the simulation time to see their correlation and contribution. In the case of hACE2, the total variance covered by the first two dimensions is almost 79.5%, where PC1 describes 63.2% and PC2 16.6%, respectively. Both the complexes (1R4L-Isoorientin and Rosavin) showed a similar pattern and positively correlated with Bond, Angle, and Vdw, in contrast to negatively correlate with coulomb. The 1R4L-Apo exhibits more or less neutral variance, and all components contributed similarly. The 1R4L-Palasitrin could be explained by PC2. In that case, the Planarity positively and Dihedral negatively correlated. The score plot and loading plot are shown in **figure 7**.

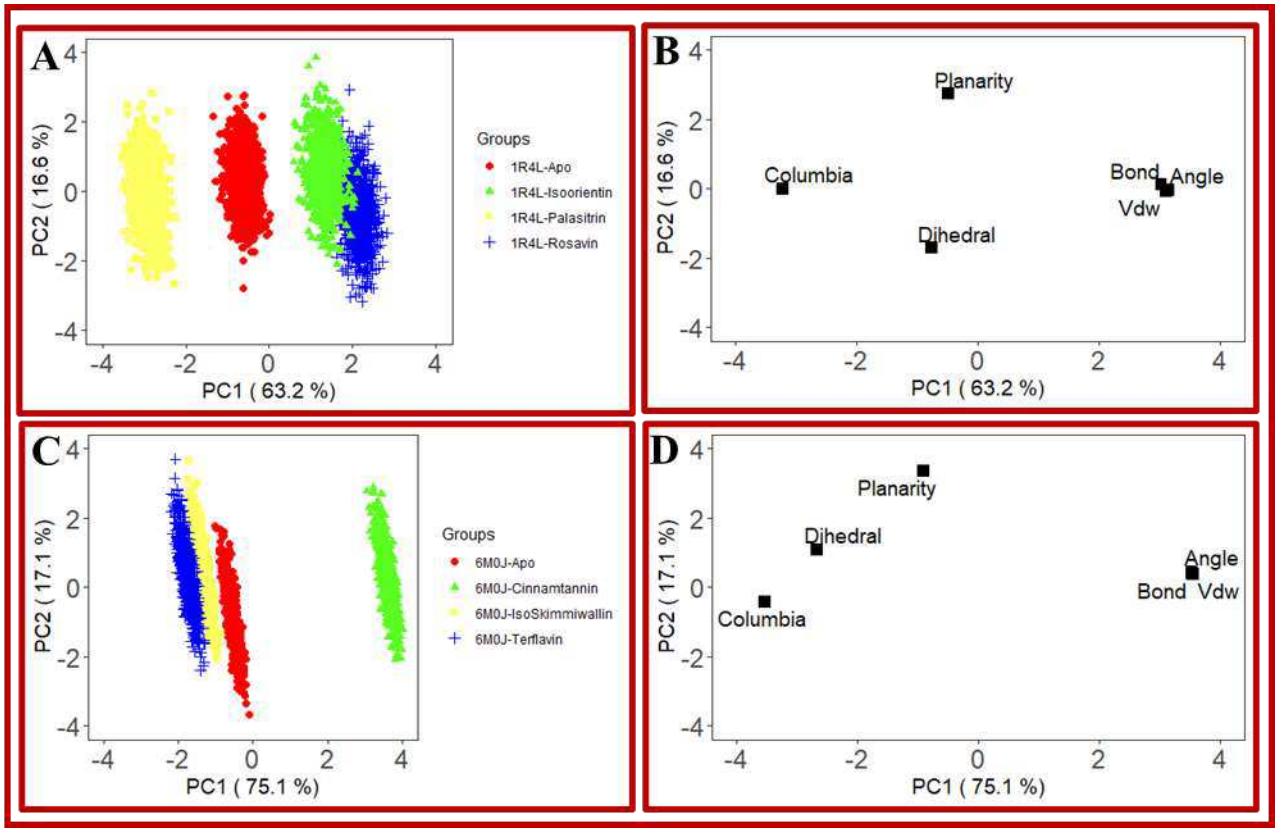

Figure 7: PCA analysis (A,C) Score plot for hACE2 and Spike-RBD (B,D) Loading plot of Apo and ligands complexes for hACE2 and Spike-RBD over 100 ns MD simulation time.

3.6. Binding free energy analysis:

The potentiality and binding affinity of the following compounds are evaluated through the estimation of binding free energy. The protein-ligand snapshots retrieved from the MD simulation trajectory were used to calculate ΔG_{bind} of both the targets 1R4L & 6M0J. In addition, the MM-PBSA approach was applied to identify the essential residues involved in the protein-ligand binding interface within the complexes. In **Figure 8 and 9**, the histogram of binding free energy (BFE) graph showed maximum negative binding energy for 1R4L: Rosavin (-383578.830 kj/mol) accompanied by Isoorientin (-370931.377) & Palasitrin (-317976.635) kj/mol respectively and for 6M0J: Cinnamtannin B1 (-199854.910 kj/mol) accompanied by IsoSkimmiwallin (-97326.808) & Terflavin A (-89497.891) kj/mol respectively. Thus, the values obtained after calculation were average free energies of binding with a more negative value indicating a stronger binding between target and ligands. The strong negative binding energy revealed that Rosavin, Isoorientin, and Palasitrin interact strongly with ACE2 receptor while, Cinnamtannin B1, IsoSkimmiwallin, and Terflavin A displayed high affinity towards S-RBD protein of SARS-CoV-2.

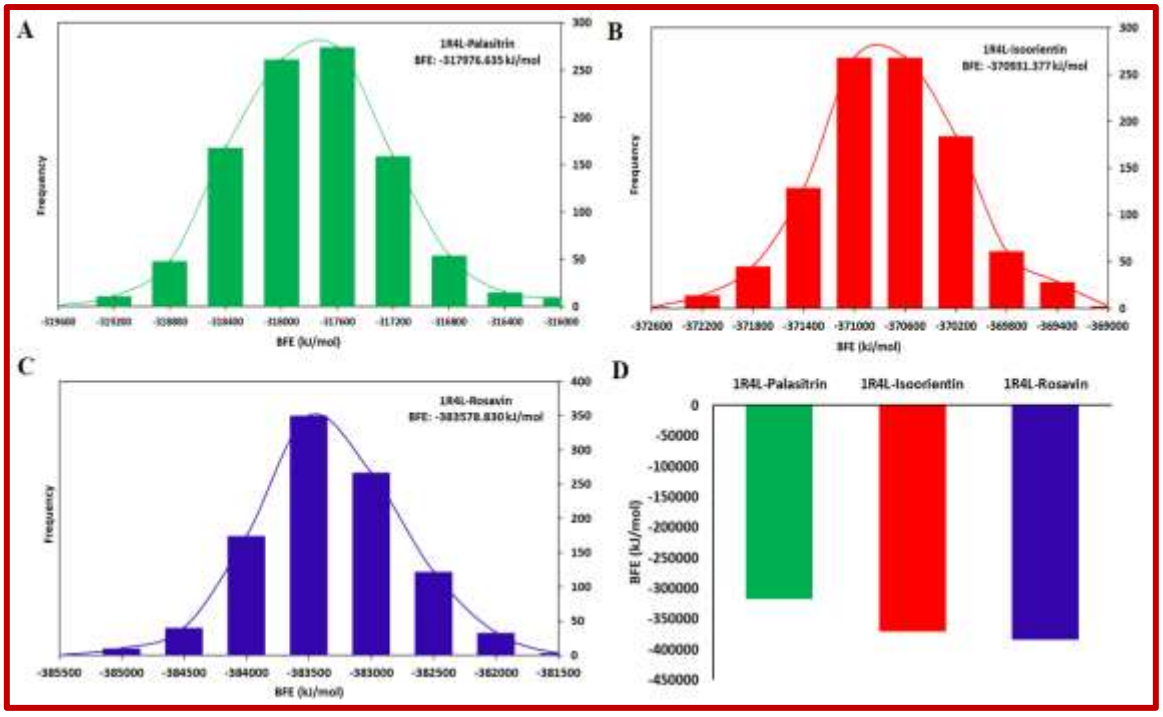

Figure 8: The histogram of binding free energy (BFE) graph for 1R4L complexes. (A) Palasitrin-green color, (B) Isoorientin-red color, (C) Rosavin-blue color, and (D) BFE comparison of all 3 complexes. The curve line represents Gaussian fit.

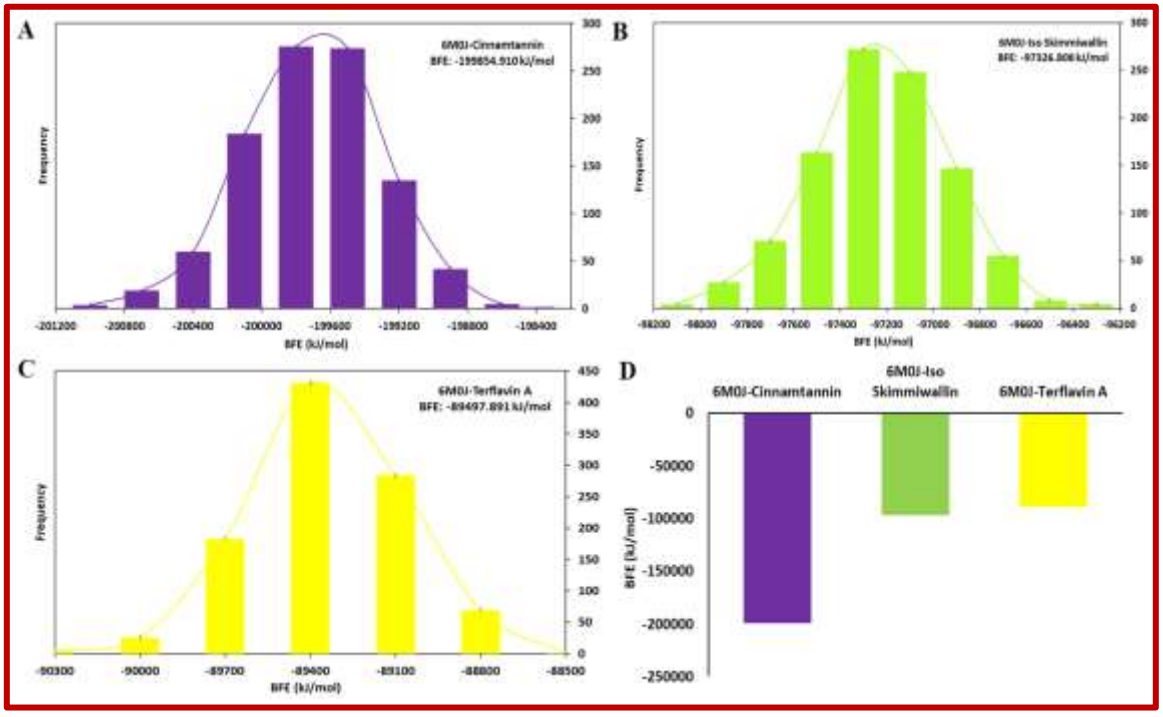

Figure 9: The histogram of binding free energy (BFE) graph for 6M0J complexes. (A) Cinnamtannin B1-violet color, (B) IsoSkimmiwallin-green color, (C) Terflavin A-yellow color, and (D) BFE comparison of all 3 complexes. The curve line represents Gaussian fit.

3.6. In-silico pharmacokinetics, drug-likeliness, and ADMET profile analysis:

The pharmacokinetics and drug likeliness of the desired molecules following several parameters' are illustrated in the following **Table 4**. The absorption, distribution, metabolism, excretion, and toxicity (ADMET) properties of these phytochemical compounds are predicted *via* the QikProp module of the Schrodinger suite. The ADMET analysis determines the physicochemical characteristics and biological properties along with the drug-likeness of the compound. It is important in terms of assessing the efficacy of drug compounds as it abruptly screens compound libraries for hits and plays a crucial role during lead optimization. Lipinski's rule of five (LoF) elucidates molecules being lead-like if it possesses a molecular weight (≤ 500Da), octanol-water partition coefficient (logP < 5), the number of H-bond donors (≤ 5), and H-bond acceptors (≤ 10), respectively. The ADMET properties of most of these phytochemicals compounds were in the satisfactory range. Some of these molecules have a large molecular weight with many stereo centres and do not follow the basic Lipinski rule of five. As per Veber's rule, which states the value of rotatable bond count (≤ 10) and PSA value (≤ 140). For target 1R4L: Eriocitrin, Rosavin, Isoorientin, Palasitrin, and Ascorbic Acid & 6M0J: Procyanidin C1, Tannic Acid, Cinnamtannin B1, Isoskimmiwallin, and Terflavin A are thus, promising lead compounds. The following descriptors such as Molecular weight, Drug-likeness, AlogP, H-bond acceptor/donor, Rotatable bonds, Polar Surface Area, Human Intestinal Absorption, Caco-2 (colorectal adenocarcinoma cells), Blood-brain barrier, Human oral bioavailability, Ames mutagenesis, Water-solubility, Plasma protein binding, Number of nitrogen & oxygen atom were predicted for the compounds. Out of these five compounds, the top three best hits for both the targets (1R4L: Rosavin, Isoorientin, and Palasitrin & 6M0J: Cinnamtannin B1, Isoskimmiwallin, and Terflavin A) are selected irrespective of some violation by taking note of other important parameters. For such compounds, structure modification and derivatization take place in such a way that it will not affect the inhibitory activity, rather improve the physicochemical properties of potent drugs. In addition, predictions of biological activities and antiviral potential were done with the use of an online computer program PASS (Prediction of Activity Spectra for Substances) which tells us that the selected compound are having similar classes of biological activities[66]. Moreover, due to biotransformation in the human body, they form one or several metabolites with different biological activity profiles. Therefore, the development and rational use of novel drugs require the analysis of their biological activity profiles, taking into account metabolism in the human body[67]. The biological activity and SAR analysis suggested that the following compounds show antiviral activity through the protease inhibitory potential with Pa ranging from 0,093 to 0,725 when Pa > Pi. These compounds are well-known antiviral for diseases like Herpes, Influenza, Hepatitis (B & C), HIV, Picornavirus, Poxvirus, and potential inhibitors of RNA-directed RNA polymerase shown in **Table 5**. Hence, from the above discussion, it is clear that the final proposed molecules are potential enough for hACE2 and S-RBD domain of SARS-CoV-2 inhibition.

Table 4: Predicted drug-likeness based on the Lipinski rule, Ghose filter, Veber rule, QED, and BBB rule.

Protein	ID	Drug	Molecular Weight (g/mol)	AlogP	H-Bond Acceptor	H-Bond Donor	Rotatable Bond	Human Intestinal Absorption	Caco-2	Blood-Brain Barrier	Human Oral Bioavailability	Ames Mutagenesis	Water Solubility (LogS)	Plasma Protein Binding (100 %)	Polar Surface Area	Nitrogen & Oxygen Atom	Rule of Five	Rule of Three
1R4L	83489	Eriocitrin	596.54	-1.46	15	9	6	0.8057	-0.9035	-0.9393	-0.8429	-0.5100	-2.772	0.894	255.5111	15	3	2
	9823887	Rosavin	428.43	-2.02	10	6	7	-0.6586	-0.8279	-0.2451	-0.6429	0.5900	-1.269	0.798	157.0004	10	1	1
	114776	Isoorientin	448.38	-0.20	11	8	3	0.8862	-0.9224	-0.6607	-0.6143	0.6100	-2.398	0.798	209.2449	11	2	2
	42607742	Palasitrin	594.52	-2.63	15	9	7	-0.426	-0.913	-0.712	-0.700	-0.540	-2.24	0.761	258.3333	15	3	2

								3	6	6	0	0	3				
	5467006 7	Ascorbic Acid	176.12	-1.41	6	4	2	0.8150	-0.9755	0.9785	0.5857	-0.9400	0.108	0.308	129.156	6	0	0
6M0J	169853	Procyanidin C1	866.78	4.44	18	15	5	0.9914	-0.8992	0.7737	-0.7857	0.6900	-3.256	0.977	327.146	18	3	2
	250395	Tannic Acid	1701.21	4.84	46	25	21	0.9147	-0.8610	-0.4403	-0.6571	-0.6600	-1.741	0.752	352.325	18	3	2
	475277	Cinnamtannin B1	864.77	4.24	18	14	4	0.9515	-0.8893	-0.2535	-0.8000	0.6200	-3.215	1.14	314.351	18	3	2
	1613037 0	Isoskimmiwallin	376.48	1.19	4	4	2	0.9755	0.8035	0.9561	-0.5714	-0.5600	-2.78	0.53	634.272	35	3	2
	1617578 8	Terflavin A	1086.74	1.98	30	17	6	0.8311	-0.8737	-0.9152	-0.5571	-0.6700	-3.035	0.536	556.187	30	3	2

Table 5: List of biological activities of best hits lead compounds for protein target 1R4L and 6M0J.

Protein	Compound Name & ID	Pa	Pi	Biological Activity
1R4L	Rosavin (9823887)	0,600	0,013	Antiviral (Influenza)
		0,490	0,011	Antiviral (Herpes)
		0,468	0,015	Antitoxic
		0,409	0,014	Antiviral (Hepatitis B)
		0,274	0,047	Antiviral
		0,205	0,066	Severe acute respiratory syndrome treatment
		0,139	0,079	Antiviral (HIV)
		0,211	0,190	Antiviral (Influenza A)
	Isoorientin (114776)	0,725	0,003	Antiviral (Herpes)
		0,709	0,005	Antiviral (Influenza)
		0,497	0,005	Antiviral (Hepatitis B)
		0,461	0,069	Antiviral (Picornavirus)
		0,391	0,004	Severe acute respiratory syndrome treatment
		0,392	0,015	Antiviral
		0,350	0,032	Antitoxic
		0,306	0,056	Antiviral (Poxvirus)
		0,171	0,022	Antiviral (Hepatitis)
		0,144	0,073	Antiviral (HIV)
		0,112	0,043	Antiviral (Hepatitis C)
		0,258	0,201	RNA-directed RNA polymerase inhibitor
		0,294	0,266	Antiviral (Rhinovirus)
		0,208	0,198	Antiviral (Influenza A)
	Palasitrin (42607742)	0,456	0,031	Antiviral (Influenza)
		0,426	0,025	Antiviral (Herpes)
		0,370	0,005	Severe acute respiratory syndrome treatment
		0,337	0,025	Antiviral (Hepatitis B)
		0,344	0,034	Antitoxic
		0,252	0,059	Antiviral
		0,141	0,077	Antiviral (HIV)
		0,255	0,205	RNA-directed RNA polymerase inhibitor
6M0J	Cinnamtannin B1 (475277)	0,436	0,058	Antiviral (Rhinovirus)
		0,369	0,050	Antiviral (Herpes)
		0,348	0,065	Antiviral (Influenza)
		0,226	0,076	Antiviral
		0,213	0,075	Antiviral (Hepatitis B)
		0,161	0,054	Antiviral (HIV)
	Terflavin A (16175788)	0,527	0,007	Antiviral (Herpes)
		0,479	0,005	Antiviral (Hepatitis B)
		0,335	0,026	Antiviral
		0,181	0,102	Severe acute respiratory syndrome treatment
		0,147	0,069	Antiviral (HIV)
		0,127	0,059	Antiviral (Hepatitis)
		0,093	0,077	Antiviral (Hepatitis C)

*__Pa:__ probability to be active; __Pi:__ probability to be inactive.

4. Discussion

With the current global cascades and its endeavour to overcome the menace and dwindle the infectious rate of COVID-19, there is an exigency for the rapid development of therapeutics medicament. However, the severity and efficacy rate of certain recent approved drugs (such as Remdesivir, Ivermectin, Lopinavir-Ritonavir, Hydroxychloroquine, etc.) for the treatment of SARS-CoV-2 has revealed the prophylaxis capacity of these medications underlying with overall adverse potential outcomes[68]. One such approved drug (Chloroquine) is used for the treatment of malaria and also, one of the prominent nanomedicines and its derivative hydroxychloroquine is being used for the treatment of coronavirus disease 2019 (COVID-19)[69]. The study reveals the safety issues with the use of these drugs for the treatment of COVID-19 in hospitalized patients (AI) and in non-hospitalized patients (AIIa) with serious heart rhythm problems including blood and lymph system disorders, kidney injuries, and liver problems & failure[70]. The federal agency of the Department of Health and Human Services (The United States Food and Drug Administration) FDA revoked the emergency use authorization (EUA) for Chloroquine and Hydroxychloroquine are unlikely to be effective in treating SARS-CoV-2 infection when a clinical trial was not feasible underlying with significant side effects[71]. The World Health Organization (WHO) does not recommend the use of Hydroxychloroquine for the treatment of COVID-19 based on six trials with more than 6000 participants[72]. Alternatively, plant-based bioactive molecules (phytochemicals) exhibit promising therapeutic efficacy against several targets of SARS-CoV-2[31]. Besides, these molecules have diverse biological properties such as antioxidant, antiviral, and anti-inflammatory activities which can be beneficial for dealing with COVID-19 virus infection[73,74]. The benefits of using natural compounds are immense as they are less toxic than synthetic drugs. Ancient Indian Scriptures including Rig-Veda [recognized three groups of plants, viz. trees (Vrksha), herbs (Osadhi), and creepers (Virudh)], Atharva-Veda, and Charaka Samhita [contains detailed descriptions of various medicinal plants] are evident of abundant medicinal benefits of plants for the treatment of various human ailments[75]. The most potent strategy of inhibiting viral entry is targeting the host or virus-related components. Therefore, a better understanding of COVID-19 pathogenesis and the structure-function relationships of drug targets will improve the success rate of new antiviral drug development. Currently, one of the most effective methods is to directly block or indirectly interfere with the interaction between SARS-CoV-2 S-protein and human ACE2. Several studies showed that plant-based bioactive molecules as potential inhibitors for structural and non-structural proteins of SARS-CoV-2 viral infection[76,77].

In the present study, human Angiotensin-Converting Enzyme 2 (hACE2) and spike receptor-binding Domain (RBD) of SARS CoV-2 are selected as a drug target for screening phytochemical having promising antiviral efficacy. The protein encoded by this gene belongs to the Angiotensin-Converting Enzyme (ACE) family of dipeptidyl carboxydipeptidases and has considerable homology to the human angiotensin 1 converting enzyme. The encoded protein is a functional receptor for the spike glycoprotein (S-domain) of the human coronavirus HCoV-NL63 and the human severe acute respiratory syndrome coronaviruses, SARS-CoV and SARS-CoV-2, the latter is the causative agent of coronavirus disease (COVID-19)[78,79].

Recent studies suggested that the binding affinity of the S-protein to the ACE2 receptor is 20 folds higher than that of SARS-CoV, as validated by Cryo-EM analysis of the spike protein structure in the perfusion conformation. According to different studies, the entry of beta-coronaviruses, such as severe acute respiratory syndrome coronavirus (SARS-CoV), the virus that causes SARS, requires binding of its spike glycoprotein, 'S-domain', to the ACE2 receptor in the body. Therefore, ACE2 and spike RBD protein have been chosen as a potential therapeutic target in this study to search drug-like plant-based molecules via multistep virtual screening-based molecular docking methods[80,81]. The lead molecule was further subjected to steered MD, MD, ADMET, and pharmacokinetic assessment. It has been observed that cells in which ACE-2 and TMPRSS2 are present were more prone to SARS-CoV-2 entry. In SARS-CoV-2 spike protein RBD there were more ACE2-interacting residues compared with SARS-CoV due to substantial mutations present in the SARS-CoV-2 sequence, more specifically in the RBD domain. ACE2 is expressed in the respiratory system, heart, intestine, kidney, and liver. Therefore, these organs are at higher risk of viral infection. Here, we have summarized the different in silico studies for the repurposing of antiviral drugs to target ACE2 and S-RBD complexes. The virtual screening of natural compounds *via* multi-step molecular docking steps followed by Glide SP and XP to the free energy binding calculation through the MM-PBSA approach led to selection of the five best hits for both the target (ACE2: Eriocitrin, Rosavin, Isoorientin, Palasitrin, and Ascorbic Acid & S-RBD: Procyanidin C1, Tannic Acid, Cinnamtannin B1, Isoskimmiwallin, and Terflavin A). In the molecular docking study, several catalytic amino acid residues were reported as important for binding interactions. The detailed molecular analysis showed that some amino acids (active site residues) were found to establish the salt bridges interaction between two groups of opposite charge compounds which plays an important role to form stable protein-ligand complexes. Several parameters such as ADMET analysis, drug likeliness, pharmacokinetics, and pharmacodynamics along with pKi, LE, Pa, and Pi are also taken into consideration to attain the supreme efficacy of the therapeutic target with minimal or no side effects. The descriptors such as Molecular weight, Drug-likeness, AlogP, H-bond acceptor/donor, Rotatable bonds, Polar Surface Area, Human Intestinal Absorption, Caco-2 (colorectal adenocarcinoma cells), Blood-brain barrier, Human oral bioavailability, Ames mutagenesis, Water-solubility, Plasma protein binding, Number of nitrogen & oxygen atom were predicted for the compounds and finally, three best hits for both the target were accounted (ACE2: Rosavin, Isoorientin, and Palasitrin & RBD: Cinnamtannin B1, Isoskimmiwallin, and Terflavin A) respectively. The binding free energy in the molecular docking for selected hits was reported in the study was in the range of -9.01 to -11.982 kcal/mol & -7.782 to -8.51 kcal/mol respectively. Mahrosh et al., 2021 also showed "Rosavin" which is an O-acyl carbohydrate extracted from the plant *Rhodiola rosea* as good antagonists against MERS-CoV (nsp13) protein which stop its proliferation in the future[82]. Pushkaran et al., 2021 demonstrated that Cinnamtannin B1 from Twak (*Cinnamomum zeylanica*) as the best binding compound against the RBD domain of spike protein[82]. The study by Rudrapal et al., 2022 revealed that "Terflavin A" as a potential drug candidate with the best binding affinity against the S-RBD receptor[82]. In present study, Fmax (pN) and Wmax (kcal/mol) calculations via steered dynamic simulation showed that Isoorientin exhibits the best performance where it asserts the

highest force value of 6871.666 pN and the highest internal work value of 1994.970 kcal/mol followed by Rosavin with the second-highest force 6082.755 pN whereas, Palasitrin displays the second highest work 1374.663 kcal/mol against Angiotensin-Converting Enzyme 2 (ACE2) protein. Similarly, IsoSkimmiwallin displays the highest work value of 337.248 kcal/mol along with the second-highest force value of 1665.646 pN followed by Terflavin A which maintains the second-highest work 249.389 kcal/mol done. Cinnamtannin depicts the highest force 1794.978 pN against spike-Receptor Binding Domain (S-RBD). Hence, based on the maximum force and work values these molecules with ACE2 and S-RBD receptor protein respectively were subjected to molecular dynamic simulation study. The RMSD, SASA, Rg and RMSA values throughout the 100 ns simulation trajectory showed stabilization of ligand protein complex with better solvent accessibility and minimum fluctuations in the amino acid residue at binding pocket of target protein. These results of PCA analysis further strengthened the stability of complex. Further, the development and rational use of novel drugs require the analysis of their biological activity profiles, and their metabolism in the human body. Furthermore, pharmacokinetic properties and antiviral activity calculated in terms of Pa and Pi ranging from 0,093 to 0,725 when Pa > Pi which suggest better druggability of lead Phyto molecules against respective targets. Our results provided strong evidence about the potential antiviral therapeutic efficacy of plant-based bioactive molecules which can block the virus-cell interaction and hence can be employed for the management and treatment of COVID-19 disease.

5. Conclusion

The interaction of hACE2 and spike RBD of SARS-CoV-2 have significant variability in infectivity and disease progression. Based on computer-assisted virtual screening and molecular docking simulation, the blockade mechanism of spike RBD and hACE2 was proposed while taking into account the highest binding activity of plant-based molecules. With this objective, the exploration of plant-based bioactive molecules using molecular docking approach against spike RBD and hACE2 respectively taken into an account to develop novel antiviral drugs that can inhibit the binding between viruses and hosts' receptors. This exploration revealed 5 potent drug molecules against both the targets (1R4L: Eriocitrin, Rosavin, Isoorientin, Palasitrin, and Ascorbic Acid) and (6M0J: Procyanidin C1, Tannic Acid, Cinnamtannin B1, Isoskimmiwallin, and Terflavin A) respectively. These lead complexes were further analyzed by SMD and MD simulation. These complexes showed stable trajectories throughout the simulation. The ADMET analysis and pharmacokinetic properties were further showed better drug likeliness of the lead molecules. Our results revealed inhibitory potential of plant-based bioactive molecules against the virus protein which can act as suitable drug for combating viral infection. However, the pre-clinical optimization of these molecules must be warranted before considering them as novel antiviral drug candidates against the SARS-CoV-2.

Acknowledgments

All authors are thankful to Mohammad A Halim for his kind suggestion and guidance throughout the research work. Also, we are grateful to The Red-Green Research Centre, Bangladesh for providing us high-Performance Computer facility for performing molecular dynamics simulation. The authors would like to thank team Schrodinger for providing the software evaluation version. Arpana Parihar is thankful to DST for providing fellowship under DST-WoS-B Scheme. The calculation of work done by Suprio is duly acknowledged. The authors extend their appreciation to the Deanship of Scientific Research at King Khalid University (KKU) for funding this research project Number (RGP.1/213/42)

Authors' Contribution

AP and RK conceptualized, designed, perform in-silico studies, wrote and proofread the manuscript. ZS perform SMD, analyzed data, and wrote SMD part. NC and PK have calculated Ki, LE, Pa, Pi, ADMET and made tables and figures, and wrote a respective part in the manuscript. IM analyzed MD data and made figures for MD and BFE and wrote the respective part. FH has done PCA and wrote the respective part. MAA performed MD simulation. MSA and AA interpreted data, wrote the manuscript and provided valuable suggestions, and proofread the manuscript. All the authors approved the final manuscript to be published.

Declarations

We confirm that this manuscript is an original work and is not under consideration by any journal.

Ethics Approval and Consent to Participate

Not applicable.

Human and Animal Rights

No humans/animals were used in the study that is the base of this research.

Consent for Publication

Not applicable.

Availability of Data and Materials

All data generated or analyzed during this study are included in this published article.

Code Availability

Not applicable

Funding

None.

Conflict of Interest

The authors declare no conflict of interest, financial or otherwise.

References

1. Hui, D. S. *et al.* The continuing 2019-nCoV epidemic threat of novel coronaviruses to global health-The latest novel coronavirus outbreak in Wuhan China. *Int J Infect Dis* **91**, 264–266 (2020).

2. Astuti, I. & Ysrafil. Severe Acute Respiratory Syndrome Coronavirus 2 (SARS-CoV-2): An overview of viral structure and host response. *Diabetes & Metabolic Syndrome* **14**, 407 (2020).

3. Alluwaimi, A. M., Alshubaith, I. H., Al-Ali, A. M. & Abohelaika, S. The Coronaviruses of Animals and Birds: Their Zoonosis, Vaccines, and Models for SARS-CoV and SARS-CoV2. *Frontiers in Veterinary Science* **7**, 582287 (2020).

4. Tracking SARS-CoV-2 variants. https://www.who.int/en/activities/tracking-SARS-CoV-2-variants/.

5. Classification of Omicron (B.1.1.529): SARS-CoV-2 Variant of Concern. https://www.who.int/news/item/26-11-2021-classification-of-omicron-(b.1.1.529)-sars-cov-2-variant-of-concern.

6. COVID-19 variants identified in the UK - GOV.UK. https://www.gov.uk/government/news/covid-19-variants-identified-in-the-uk.

7. Rodriguez-Palacios, A. *et al.* Comparative Review of SARS-CoV-2, SARS-CoV, MERS-CoV, and Influenza A Respiratory Viruses. *Frontiers in Immunology | www.frontiersin.org* **1**, 552909 (2019).

8. Lu, R. *et al.* Genomic characterisation and epidemiology of 2019 novel coronavirus: implications for virus origins and receptor binding. *The Lancet* **395**, 565–574 (2020).

9. Xia, B. *et al.* SARS-CoV-2 envelope protein causes acute respiratory distress syndrome (ARDS)-like pathological damages and constitutes an antiviral target. *Cell Research* doi:10.1038/s41422-021-00519-4.

10. WHO Coronavirus (COVID-19) Dashboard | WHO Coronavirus (COVID-19) Dashboard With Vaccination Data. https://covid19.who.int/.

11. Khan, M. T. *et al.* Immunoinformatics and molecular modeling approach to design universal multi-epitope vaccine for SARS-CoV-2. *Informatics in Medicine Unlocked* **24**, 100578 (2021).

12. Yadav, R. *et al.* Role of Structural and Non-Structural Proteins and Therapeutic Targets of SARS-CoV-2 for COVID-19. *Cells 2021, Vol. 10, Page 821* **10**, 821 (2021).

13. Naqvi, A. A. T. *et al.* Insights into SARS-CoV-2 genome, structure, evolution, pathogenesis and therapies: Structural genomics approach. *Biochimica et Biophysica Acta - Molecular Basis of Disease* **1866**, (2020).

14. Fehr, A. R. & Perlman, S. Chapter 1 Coronaviruses: An Overview of Their Replication and Pathogenesis. *Methods in Molecular Biology* **1282**,.

15. McBride, R., van Zyl, M. & Fielding, B. C. The coronavirus nucleocapsid is a multifunctional protein. *Viruses* **6**, 2991–3018 (2014).

16. Ni, W. *et al.* Role of angiotensin-converting enzyme 2 (ACE2) in COVID-19. *Critical Care* **24**, 1–10 (2020).

17. Wiese, O., Zemlin, A. E. & Pillay, T. S. Molecules in pathogenesis: angiotensin converting enzyme 2 (ACE2). *Journal of Clinical Pathology* **74**, 285–290 (2021).

18. Zhang, Q. *et al.* Molecular mechanism of interaction between SARS-CoV-2 and host cells and interventional therapy. *Signal Transduction and Targeted Therapy 2021 6:1* **6**, 1–19 (2021).

19. Jackson, C. B., Farzan, M., Chen, B. & Choe, H. Mechanisms of SARS-CoV-2 entry into cells. *Nature Reviews Molecular Cell Biology 2021 23:1* **23**, 3–20 (2021).

20. Huang, Y., Yang, C., Xu, X. feng, Xu, W. & Liu, S. wen. Structural and functional properties of SARS-CoV-2 spike protein: potential antivirus drug development for COVID-19. *Acta Pharmacologica Sinica 2020 41:9* **41**, 1141–1149 (2020).

21. Belouzard, S., Millet, J. K., Licitra, B. N. & Whittaker, G. R. Mechanisms of Coronavirus Cell Entry Mediated by the Viral Spike Protein. *Viruses 2012, Vol. 4, Pages 1011-1033* **4**, 1011–1033 (2012).

22. Rahbar Saadat, Y., Hosseiniyan Khatibi, S. M., Zununi Vahed, S. & Ardalan, M. Host Serine Proteases: A Potential Targeted Therapy for COVID-19 and Influenza. *Frontiers in Molecular Biosciences* **8**, 816 (2021).

23. Haque, S. K. M., Ashwaq, O., Sarief, A. & Azad John Mohamed, A. K. A comprehensive review about SARS-CoV-2. *Future Virology* **15**, 625–648 (2020).

24. Salamanna, F., Maglio, M., Landini, M. P. & Fini, M. Body Localization of ACE-2: On the Trail of the Keyhole of SARS-CoV-2. *Frontiers in Medicine* **7**, 935 (2020).

25. Horowitz, R. I. & Freeman, P. R. Three novel prevention, diagnostic, and treatment options for COVID-19 urgently necessitating controlled randomized trials. *Medical Hypotheses* **143**, 109851 (2020).

26. Dash, P., Mohapatra, S., Ghosh, S. & Nayak, B. A Scoping Insight on Potential Prophylactics, Vaccines and Therapeutic Weaponry for the Ongoing Novel Coronavirus (COVID-19) Pandemic- A Comprehensive Review. *Frontiers in Pharmacology* **11**, 2471 (2021).

27. Sultan, M. T., Buttxs, M. S., Qayyum, M. M. N. & Suleria, H. A. R. Immunity: Plants as Effective Mediators. *https://doi.org/10.1080/10408398.2011.633249* **54**, 1298–1308 (2014).

28. Rollinger, J. M., Stuppner, H. & Langer, T. Virtual screening for the discovery of bioactive natural products. *Progress in Drug Research* **65**, 211–249 (2008).

29. Singh Jadoun, S., Chand Mali, P. & Kumar Choudhary, N. A Review on Immunity Boosting by Herbal Medicines to Cure and Treatment of Covid-19 Affects. **07**, 3–8 (2021).

30. Naik, B. *et al.* High throughput virtual screening reveals SARS-CoV-2 multi-target binding natural compounds to lead instant therapy for COVID-19 treatment. *International Journal of Biological Macromolecules* **160**, 1–17 (2020).

31. Parihar, A. *et al.* Phytochemicals-based targeting RdRp and main protease of SARS-CoV-2 using docking and steered molecular dynamic simulation: A promising therapeutic approach for Tackling COVID-19. *Computers in Biology and Medicine* 105468 (2022) doi:10.1016/J.COMPBIOMED.2022.105468.

32. Ebob, O. T., Babiaka, S. B. & Ntie-Kang, F. Natural Products as Potential Lead Compounds for Drug Discovery Against SARS-CoV-2. *Natural Products and Bioprospecting* **11**, 611–628 (2021).

33. Mishra, P., Sohrab, S. & Mishra, S. K. A review on the phytochemical and pharmacological properties of Hyptis suaveolens (L.) Poit. *Future Journal of Pharmaceutical Sciences* **7**, 1–11 (2021).

34. Parihar, A., Puranik, N., Khandia, R. & Khan, R. Phytochemicals based therapeutic approaches for Breast cancer targeting: Molecular docking study. (2022) doi:10.26434/CHEMRXIV-2022-K7GS1.

35. Singh, P. *et al.* The dual role of phytochemicals on SARS-CoV-2 inhibition by targeting host and viral proteins. *Journal of Traditional and Complementary Medicine* **12**, 90–99 (2022).

36. Meng, X.-Y., Zhang, H.-X., Mezei, M. & Cui, M. Molecular Docking: A powerful approach for structure-based drug discovery. *Curr Comput Aided Drug Des* **7**, 146 (2011).

37. Majumder, R. & Mandal, M. Screening of plant-based natural compounds as a potential COVID-19 main protease inhibitor: an in silico docking and molecular dynamics simulation approach. *Journal of Biomolecular Structure and Dynamics* **40**, 696–711 (2022).

38. Hughes, J. P., Rees, S. S., Kalindjian, S. B. & Philpott, K. L. Principles of early drug discovery. *British Journal of Pharmacology* **162**, 1239–1249 (2011).

39. Lionta, E., Spyrou, G., Vassilatis, D. & Cournia, Z. Structure-Based Virtual Screening for Drug Discovery: Principles, Applications and Recent Advances. *Current Topics in Medicinal Chemistry* **14**, 1923–1938 (2014).

40. PubChem. https://pubchem.ncbi.nlm.nih.gov/.

41. Shelley, J. C. *et al.* Epik: A software program for pKa prediction and protonation state generation for drug-like molecules. *Journal of Computer-Aided Molecular Design* **21**, 681–691 (2007).

42. RCSB PDB: Homepage. https://www.rcsb.org/.

43. Madhavi Sastry, G., Adzhigirey, M., Day, T., Annabhimoju, R. & Sherman, W. Protein and ligand preparation: Parameters, protocols, and influence on virtual screening enrichments. *Journal of Computer-Aided Molecular Design* **27**, 221–234 (2013).

44. Olawale, F., Iwaloye, O. & Elekofehinti, O. O. Virtual screening of natural compounds as selective inhibitors of polo-like kinase-1 at C-terminal polo box and N-terminal catalytic domain. *Journal of Biomolecular Structure and Dynamics* (2021) doi:10.1080/07391102.2021.1991476/SUPPL_FILE/TBSD_A_1991476_SM6773.DOCX.

45. Mittal, L., Kumari, A., Srivastava, M., Singh, M. & Asthana, S. Identification of potential molecules against COVID-19 main protease through structure-guided virtual screening approach. *Journal of Biomolecular Structure and Dynamics* **39**, 3662–3680 (2021).

46. Parihar, A. *et al.* In silico analysis for the repurposing of broad-spectrum antiviral drugs against multiple targets from SARS-CoV-2: A molecular docking and ADMET approach. (2022) doi:10.21203/rs.3.rs-1242644/v1.

47. Halgren, T. A. *et al.* Glide: A New Approach for Rapid, Accurate Docking and Scoring. 2. Enrichment Factors in Database Screening. *Journal of Medicinal Chemistry* **47**, 1750–1759 (2004).

48. Ioakimidis, L., Thoukydidis, L., Mirza, A., Naeem, S. & Reynisson, J. Benchmarking the reliability of QikProp. correlation between experimental and predicted values. *QSAR and Combinatorial Science* **27**, 445–456 (2008).

49. Forouzesh, N., Mishra, N. An Effective MM / GBSA Protocol for Absolute Binding Free. *Molecules* **26**, (2021).

50. Mohammad, T. *et al.* Identification of high-affinity inhibitors of SARS-CoV-2 main protease: Towards the development of effective COVID-19 therapy. *Virus Research* **288**, 198102 (2020).

51. Krieger, E., Dunbrack, R. L., Hooft, R. W. W. & Krieger, B. Assignment of Protonation States in Proteins and Ligands: Combining pK<Subscript>a</Subscript> Prediction with Hydrogen Bonding Network Optimization. *Methods in Molecular Biology* **819**, 405–421 (2012).

52. Dickson, C. J. *et al.* Lipid14: The amber lipid force field. *Journal of Chemical Theory and Computation* **10**, 865–879 (2014).

53. Khan, S. *et al.* Structure-based identification of potential SARS-CoV-2 main protease inhibitors. *Journal of Biomolecular Structure and Dynamics* (2020) doi:10.1080/07391102.2020.1848634/SUPPL_FILE/TBSD_A_1848634_SM5212.DOCX.

54. Sakib, M. M. H. *et al.* Computational screening of 645 antiviral peptides against the receptor-binding domain of the spike protein in SARS-CoV-2. *Computers in Biology and Medicine* **136**, 104759 (2021).

55. Krieger, E. & Vriend, G. New ways to boost molecular dynamics simulations. *Journal of Computational Chemistry* **36**, 996–1007 (2015).

56. Kollman, P. A. *et al.* Calculating Structures and Free Energies of Complex Molecules: Combining Molecular Mechanics and Continuum Models. *Accounts of Chemical Research* **33**, 889–897 (2000).

57. Hou, T., Wang, J., Li, Y. & Wang, W. Assessing the performance of the MM/PBSA and MM/GBSA methods. 1. The accuracy of binding free energy calculations based on molecular dynamics simulations. *Journal of Chemical Information and Modeling* **51**, 69–82 (2011).

58. Hayes, J. M. & Archontis, G. MM-GB(PB)SA Calculations of Protein-Ligand Binding Free Energies. *Molecular Dynamics - Studies of Synthetic and Biological Macromolecules* (2012) doi:10.5772/37107.

59. Yang, H. *et al.* AdmetSAR 2.0: Web-service for prediction and optimization of chemical ADMET properties. *Bioinformatics* **35**, 1067–1069 (2019).

60. Daina, A., Michielin, O. & Zoete, V. SwissADME: a free web tool to evaluate pharmacokinetics, drug-likeness and medicinal chemistry friendliness of small molecules. *Scientific Reports 2017 7:1* **7**, 1–13 (2017).

61. Veber, D. F. *et al.* Molecular properties that influence the oral bioavailability of drug candidates. *Journal of Medicinal Chemistry* **45**, 2615–2623 (2002).

62. Lipinski, C. A., Lombardo, F., Dominy, B. W. & Feeney, P. J. Experimental and computational approaches to estimate solubility and permeability in drug discovery and development settings. *Advanced Drug Delivery Reviews* **64**, 4–17 (2012).

63. De Vrieze, M., Janssens, P., Szucs, R., Van der Eycken, J. & Lynen, F. In vitro prediction of human intestinal absorption and blood–brain barrier partitioning: Development of a lipid analog for micellar liquid chromatography. *Analytical and Bioanalytical Chemistry* **407**, 7453–7466 (2015).

64. Abbott, N. J. Physiology of the blood–brain barrier and its consequences for drug transport to the brain. *Int Congr Ser* **1277**, 3–18 (2005).

65. Shukla, R. & Tripathi, T. Molecular Dynamics Simulation of Protein and Protein–Ligand Complexes. *Computer-Aided Drug Design* 133–161 (2020) doi:10.1007/978-981-15-6815-2_7.

66. Way2Drug - main. http://way2drug.com/passonline/index.php.

67. Filimonov, D. A., Rudik, A. V., Dmitriev, A. V. & Poroikov, V. V. Computer-Aided Estimation of Biological Activity Profiles of Drug-Like Compounds Taking into Account Their Metabolism in Human Body. *International Journal of Molecular Sciences 2020, Vol. 21, Page 7492* **21**, 7492 (2020).

68. Magro, G. COVID-19: Review on latest available drugs and therapies against SARS-CoV-2. Coagulation and inflammation cross-talking. *Virus Research* **286**, 198070 (2020).

69. Davidescu, E. I. *et al.* Treatment with hydroxychloroquine in patients with covid-19. Experience of a neurology department. *Farmacia* **68**, 597–605 (2020).

70. FDA cautions against use of hydroxychloroquine or chloroquine for COVID-19 outside of the hospital setting or a clinical trial due to risk of heart rhythm problems | FDA. https://www.fda.gov/drugs/drug-safety-and-availability/fda-cautions-against-use-hydroxychloroquine-or-chloroquine-covid-19-outside-hospital-setting-or.

71. Coronavirus (COVID-19) Update: FDA Revokes Emergency Use Authorization for Chloroquine and Hydroxychloroquine | FDA. https://www.fda.gov/news-events/press-announcements/coronavirus-covid-19-update-fda-revokes-emergency-use-authorization-chloroquine-and.

72. Coronavirus disease (COVID-19): Hydroxychloroquine. https://www.who.int/news-room/questions-and-answers/item/coronavirus-disease-(covid-19)-hydroxychloroquine.

73. Parham, S. *et al.* Antioxidant, antimicrobial and antiviral properties of herbal materials. *Antioxidants* **9**, 1–36 (2020).

74. Mukhtar, M. *et al.* Antiviral potentials of medicinal plants. *Virus Research* **131**, 111 (2008).

75. Balkrishna, A. *et al.* Ancient Indian rishi's (Sages) knowledge of botany and medicinal plants since Vedic period was much older than the period of Theophrastus, A case study-who was the actual father of botany? *40 ~ International Journal of Unani and Integrative Medicine* **3**, 40–44 (2019).

76. Bhuiyan, F. R., Howlader, S., Raihan, T. & Hasan, M. Plants Metabolites: Possibility of Natural Therapeutics Against the COVID-19 Pandemic. *Frontiers in Medicine* **7**, 444 (2020).

77. Kumar, A. *et al.* Identification of phytochemical inhibitors against main protease of COVID-19 using molecular modeling approaches. (2020) doi:10.21203/RS.3.RS-31210/V1.

78. Hofmann, H. *et al.* Highly Conserved Regions within the Spike Proteins of Human Coronaviruses 229E and NL63 Determine Recognition of Their Respective Cellular Receptors. *Journal of Virology* **80**, 8639–8652 (2006).

79. Li, W. *et al.* The S proteins of human coronavirus NL63 and severe acute respiratory syndrome coronavirus bind overlapping regions of ACE2. *Virology* **367**, 367–374 (2007).

80. Brown, E. E. F. *et al.* Characterization of Critical Determinants of ACE2-SARS CoV-2 RBD Interaction. *Int J Mol Sci* **22**, 1–15 (2021).

81. Abubakar, M. B. *et al.* Natural Products Modulating Angiotensin Converting Enzyme 2 (ACE2) as Potential COVID-19 Therapies. *Frontiers in Pharmacology* **12**, 629935 (2021).

82. Rudrapal, M. *et al.* Identification of bioactive molecules from Triphala (Ayurvedic herbal formulation) as potential inhibitors of SARS-CoV-2 main protease (Mpro) through computational investigations. *Journal of King Saud University - Science* **34**, 101826 (2022).